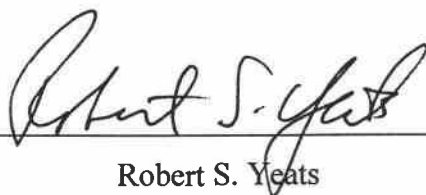# AN ABSTRACT OF THE THESIS OF

Daniel J. Myers for the degree of Master of Science in Geology presented on June 5, 2001. Title: Structural Geology and Dislocation Modeling of the East Coyote Anticline, Eastern Los Angeles Basin

Abstract approved: _____

Robert S. Yeats

The 1994 Northridge and 1987 Whittier Narrows earthquakes warned Los Angeles residents of the threat of earthquakes due to unmapped, blind reverse faults and emphasized the importance of identifying and characterizing blind reverse faults in assessing the seismic hazard to the region. The East and West Coyote Hills in the eastern Los Angeles basin are the surface expression of uplift accompanying blind reverse faulting. Folded Quaternary strata indicate that the hills are growing and that the faults underlying them are active. We use oil well data from the oil field beneath the East Coyote Hills to characterize the deformation. Detailed subsurface mapping in the East Coyote oil field shows that a previously-mapped, reverse-separation fault that cuts wells in the field is predominantly an inactive strike-slip fault that is not responsible for the uplift of the East Coyote Hills. The fault responsible for folding the East and West Coyote oil fields and the uplift of the Coyote Hills does not cut wells in either oil field. To characterize the geometry of the blind fault responsible for folding, we employ dislocation modeling. The dip and upper fault tip depths obtained from modeling suggest that the thrust fault beneath the Coyote Hills fault may be an extension of the Puente Hills blind thrust fault. The Coyote Hills fault is part of a major crustal structure that underlies much of the northern Los Angeles basin, with important implications for the tectonics and earthquake hazards of the Los Angeles basin. Modeling results suggest that the thrust fault responsible for folding would have 1400 m of reverse displacement over the last 1.2 Ma. This yields an average slip rate of $1.2\ ^{+1.4}/_{-0.5}$ mm/yr for this time

interval. Estimated moment magnitude for a reverse displacement earthquake on the Coyote Hills blind fault ranges from 6 to 7 depending on the length of the rupture. The average earthquake recurrence interval is 730 – 4000 years based on slip rates of 1.2 mm/yr and 0.8 mm/yr.

Structural Geology and Dislocation Modeling of the East Coyote Anticline, Eastern Los Angeles Basin

By Daniel J. Myers
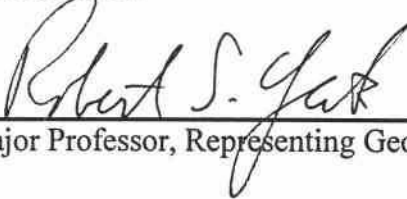
A THESIS

Submitted to

Oregon State University

In partial fulfillment of
the requirements for the
degree of

Master of Science

Presented on June 5, 2001
Commencement June, 2002

Master of Science thesis by Daniel J. Myers presented on June 5, 2001

APPROVED:

_____

Major Professor, Representing Geology

_____

Chair of Department of Geosciences

_____

Dean of Graduate School

I understand that my thesis will become part of the permanent collection of Oregon State University libraries. My signature below authorizes release of my thesis to any reader upon request.

_____

Daniel J. Myers, Author

ACKNOWLEDGMENTS

TABLE OF CONTENTS

LIST OF FIGURES

Structural Geology and Dislocation Modeling of the East Coyote Anticline, Eastern Los Angeles Basin

INTRODUCTION

In recent years, much of the earthquake hazards research in the Los Angeles basin of California has focused on locating active blind thrusts. This is a result of the 1987 Whittier Narrows and 1994 Northridge earthquakes that occurred on previously unrecognized blind thrust faults and caused extensive damage in metropolitan Los Angeles. Identifying and characterizing blind thrust faults is difficult because the faults do not reach the surface. Seismic, topographic, or well data are required to locate and constrain the geometries of these faults. One of these blind thrust faults underlies the Coyote Hills in the eastern Los Angeles Basin.

The Coyote Hills are the topographic expression of folding of strata as young as late Quaternary, indicating that deformation is ongoing. If the Coyote Hills fold is generated by a blind reverse fault, then this fault could represent a significant earthquake hazard. Characterizing the nature of the deformation of the East Coyote Hills is used to understand deformation of the Coyote Hills and other nearby structures.

Other workers (Shaw and Shearer, 1999; Fuis and others, 2001) have suggested that a blind thrust fault (Puente Hills blind thrust) underlies the northern Los Angeles basin west of the Coyote Hills. The structure underlying the Coyote Hills may be related to the Puente Hills blind thrust.

The goals of this paper are to (1) describe the important subsurface structural features of the Coyote Hills focusing on the East Coyote Hills, (2) determine the timing and mechanism of active folding of the East Coyote Hills, (3) integrate the structure of the Coyote Hills into the existing Los Angeles Basin tectonic framework, (4) estimate the slip rate on the blind reverse fault generating the Coyote Hills, and (5) estimate the magnitude and recurrence interval of an earthquake on the Coyote Hills blind thrust, assuming the entire blind fault ruptures in a single earthquake. We determine the subsurface geologic structure using surface mapping, oil-industry well logs, oil-field reports, and proprietary seismic reflection data. Based on this structure, we then

investigate the mechanism and rate of folding using dislocation modeling to re-create the folding of a Quaternary contact in the subsurface. This allows an estimate of the size, geometry and slip on an active blind thrust beneath the Coyote Hills. Paleomagnetic and tephrochronologic age constraints on the folded Quaternary surface permit the estimation of slip rates. We also explore some of the inherent limitations of dislocation modeling for constraining blind thrust fault geometry.

TECTONIC SETTING

The Coyote Hills lie in the eastern Los Angeles basin on the north side of the city of Fullerton, 36 km east-southeast of downtown Los Angeles. The Coyote Hills are subdivided into the East Coyote Hills and the West Coyote Hills. The eastern edge of the West Coyote Hills is 1.2 km west of the East Coyote Hills with an en-échelon right step in the topography. Both sets of hills have oil fields beneath them (Figure 1a). The East Coyote oil field is divided into two structural domes; the Hualde dome in the western part of the field, and the Anaheim dome in the eastern part of the field.

Several active geologic structures are located near the Coyote Hills (Figure 1a). The dextral-oblique slip Whittier fault, 5 km to the northeast in the foothills of the Puente Hills, strikes west-northwest near the southern edge of the Puente Hills. The Coyote Hills trend merges eastward with the Whittier fault beyond the Richfield and Kraemer anticlines, each underlain by an oil field.

West of the Coyote Hills is the south-vergent, blind Carmenita thrust, which is the near-surface expression of the Puente Hills blind thrust of Shaw and Shearer (1999) that produced the 1987 Whittier Narrows earthquake. The Santa Fe Springs oil field is within the hanging wall of the Carmenita thrust. The west-northwest-striking La Habra syncline lies between the Coyote Hills and the Puente Hills. The La Habra syncline appears to be active because Quaternary strata in the syncline show syntectonic thickening (Figures 2a and b). To the south, the Anaheim Nose contains deformed rocks as young as Pliocene (Figures 2a and b). Quaternary strata imaged on oil industry seismic reflection lines, however, do not thin across the crest of the anticline and are not folded, indicating that the Anaheim nose is no longer growing.
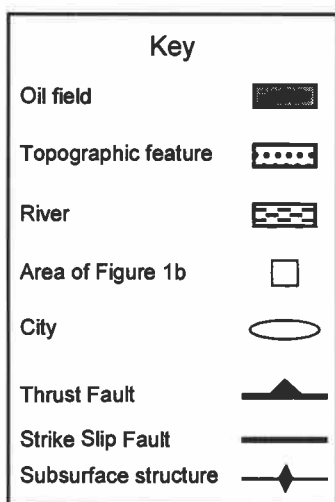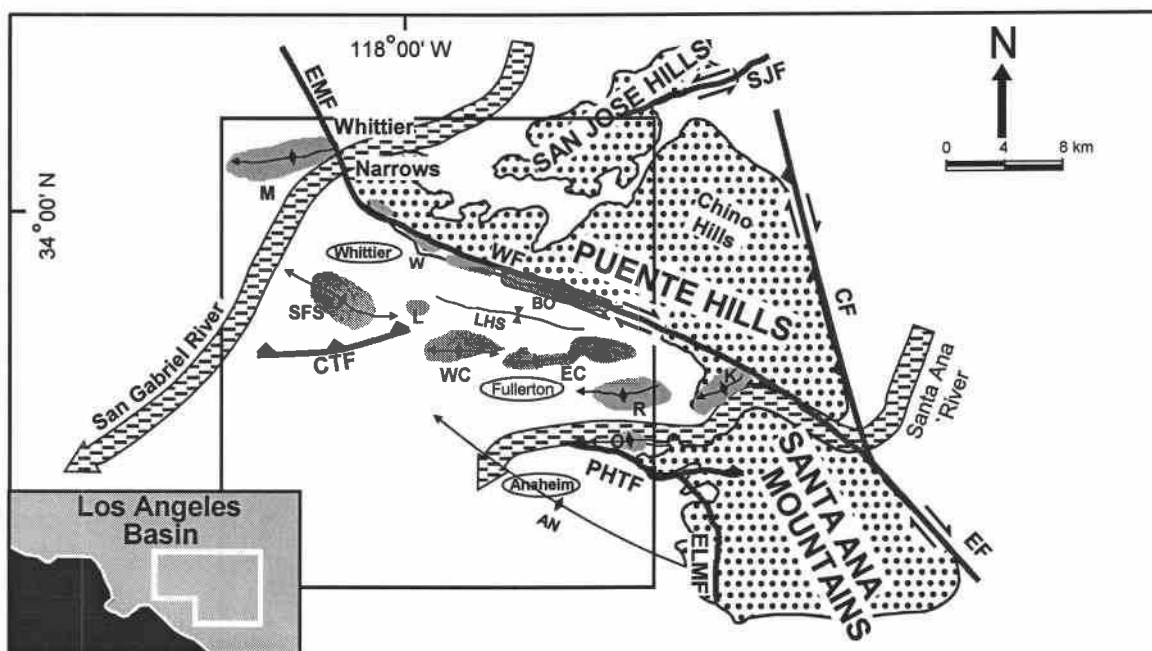
Figure 1: a) Location of the Coyote oil fields and important geologic structures. Abbreviations are as follows: Faults (CF – Chino fault, CTF – Carmenita thrust fault, EF – Elsinore fault, ELMF – El Modeno fault, EMF – East Montebello fault, PHTF – Peralta Hills thrust fault, SJF – San Jose fault, WF – Whittier fault), Oil fields (BO -Brea-Olinda, EC – East Coyote, K - Kraemer, L – Leffingwell, M – Montebello, O – Olive, R – Richfield, SFS – Santa Fe Springs, W – Whittier, WC – West Coyote), Structures (AN – Anaheim nose, LHS – La Habra syncline). Ellipses contain city names. Data compiled from Gray (1961), Yerkes and others (1965) and Wright (1991) by Eldon Gath of Earth Consultants International.

Key

Oil field	
Topographic feature	
River	
Area of Figure 1b	
City	
Thrust Fault	
Strike Slip Fault	
Subsurface structure	
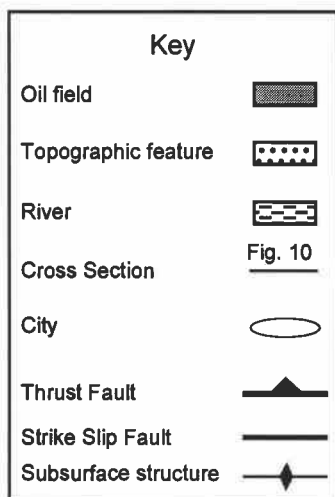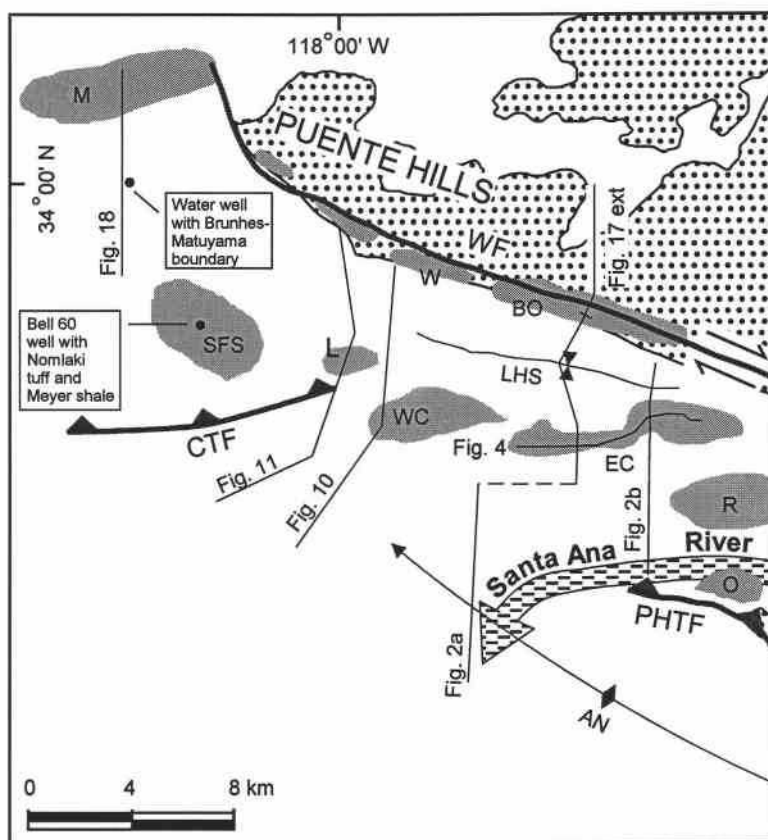
Figure 1: b) Location of cross sections, Brunhes-Matuyama magnetic chron boundary, and Nomlaki tuff. Brunhes-Matuyama boundary location from Ponti (pers. comm., 1999), and Nomlaki tuff location from A. Sarna-Wojcicki (pers. comm., 2000).
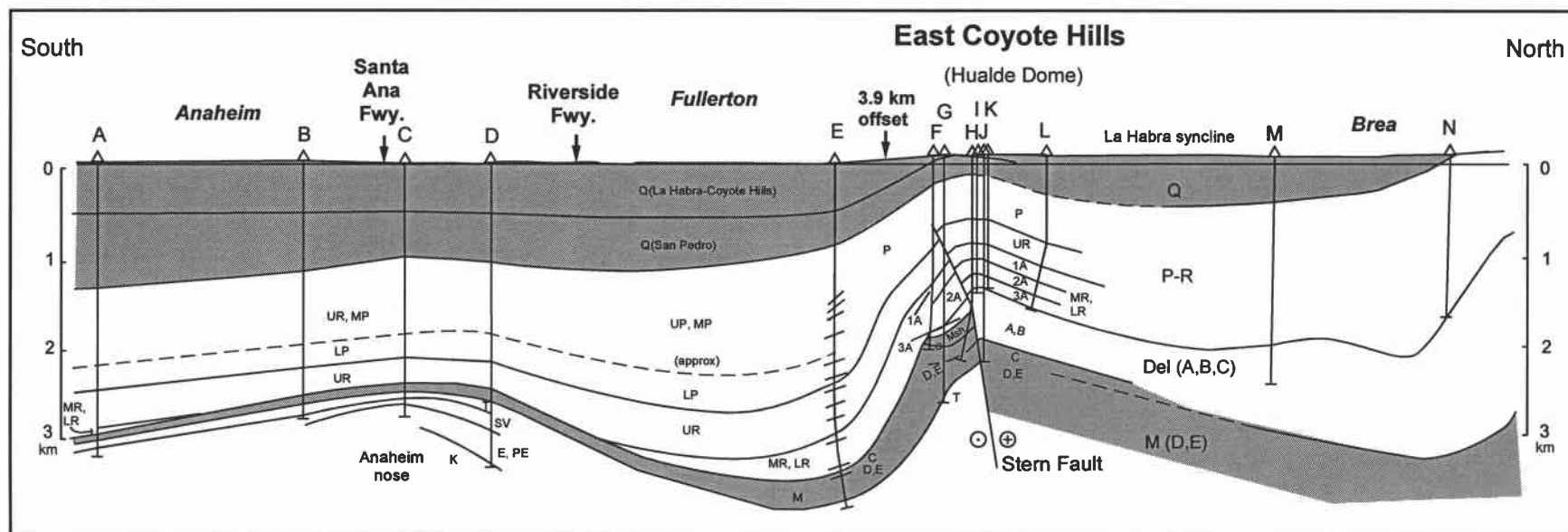
Figure 2: a) North-south cross section from the city of Brea to the Anaheim nose through the Hualde dome of the East Coyote oil field. The section shows features consistent with strike-slip offset on the Stern fault. The top of the Upper Repetto (UR) shows reverse separation, while the top of the Stern zone (Miocene C) shows normal separation. The 2nd Anaheim (2A) zone shows an abrupt increase in thickness across the Stern fault, and the thick "Delmontian" strata (A, B) north of the fault have no equivalents on the south of the fault. Quaternary strata are not folded in the Anaheim nose, indicating that it is a dead structure.

Unit name abbreviations: Q – Quaternary; P – Pico (U – upper, M – middle, L – lower); R – Repetto; 1A – 1st Anaheim zone; 2A – 2nd Anaheim zone; 3A – 3rd Anaheim zone; Msh – Mohnian shale; A, B, C, D, E – Miocene divisions of Wissler (1958); Del – local "Delmontian" stage; M – Mohnian stage; St – Stern zone; T – Topanga; SV – Sespe-Vaqueros; E, PE – Eocene, Paleocene; K – Upper Cretaceous. Names of cities in italics. Wells identified in appendix.
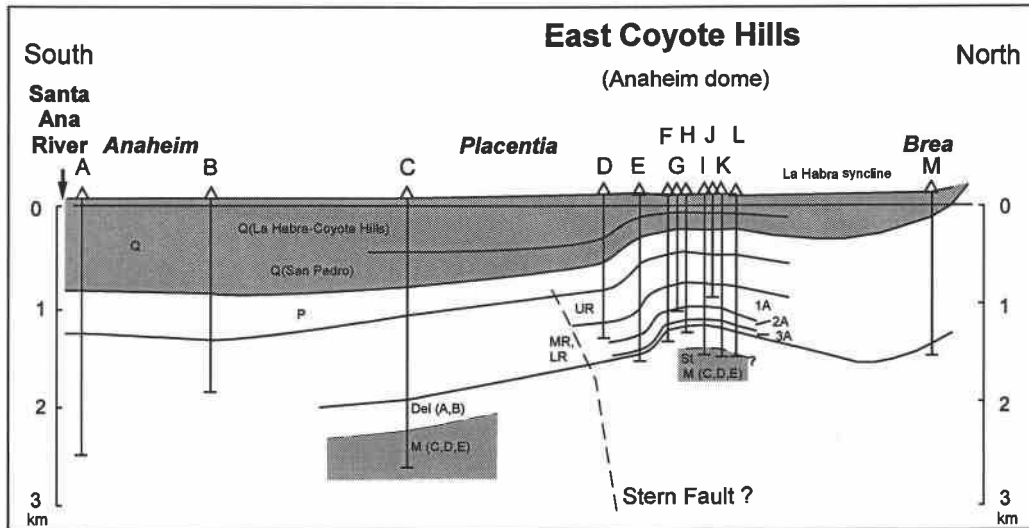
Figure 2: b) North-south cross section through the Anaheim dome of the East Coyote oil field. There is no fault on the south flank of the Anaheim dome; the Stern fault may lie between wells C and D. The Anaheim dome is less strongly folded than the Hualde dome. Relief on the base San Pedro surface is approximately 600 meters for the Anaheim dome as compared to approximately 1000 meters for the Hualde dome. The Pico thins to a much greater extent across the Hualde dome than across the Anaheim dome.

Unit name abbreviations the same as for figure 2a.

STRATIGRAPHY

In order to determine the subsurface structure of the East Coyote Hills, we mapped subsurface rock units using self-potential and resistivity logs from oil industry wells. Figure 3 shows a type log for the East Coyote Hills, with ages of the stratigraphic boundaries from Blake (1991). The oldest rocks reached by wells in the East Coyote oil field are early to middle Miocene Topanga Group, which includes massive, coarse-grained sandstone interbedded with sandy shale and siltstone (Blake, 1991). The Topanga Group is overlain by siltstone and sandstone of the Puente Formation. This contact is unconformable in the Puente Hills (Blake, 1991). So few wells in the East Coyote Hills oil field reach this contact that we cannot comment on its nature in the subsurface of the East Coyote Hills, and therefore we do not include the Topanga Group on the type log. Rocks of the Puente Formation include the Mohnian and "Delmontian" benthic foraminiferal stages of Kleinpell (1938). These are further subdivided into the Mohnian C, D, and E divisions of Wissler (1958) and "Delmontian" A and B divisions of Wissler (1958). The "Delmontian" of the Los Angeles basin is not the same age as the type Delmontian in the central Coast Ranges, and so it is used here in quotes with local age range from Blake (1991). Where reached by wells within the East Coyote Hills, the Miocene Division C strata are subdivided into the sandstone of the Stern zone and an overlying Mohnian shale. The sandstone of the Stern zone continues downsection into the D and E divisions of Wissler (1958). The contact between the "Delmontian" and Mohnian strata appears to be an angular unconformity in the Hualde dome of the East Coyote oil field (Figures 2a and 4).

The "Delmontian" stata are overlain conformably by the Pliocene Repetto Member of the Fernando Formation. The "Delmontian" strata lens out to the west, so that wells in the westernmost portion of the East Coyote field show lower Repetto directly on Mohnian strata (Figures 4 and 5b). Sandstone and shale of the Repetto

Epoch	Benthic Foram Stage	Division	Formation	Oil-producing Zone	Type Log (depths in feet)	Lithologic Description	Approximate Age (Ma)*
Pleistocene	Hallian		La Habra/Coyote Hills Undiff.		500	Nonmarine sandstone, silty conglomerate, and siltstone*	
Pleistocene	Hallian		San Pedro		1000	Nonmarine to inner-neritc siltstone, sandstone, claystone and conglomerate* Contains magnetic chron boundary midway in section (780 ± 10 ka based on Spell and others, 1992) **Modeled Surface**	1?
Pliocene	Whee-lerian		Pico		1500	Neritic to middle bathyal siltstone, claystone, silty sands, and shales*	2
Pliocene	Venturian		Pico		2000		
Pliocene	Repettian	Fernando / Repetto	Upper		2500 / 3000	Approximate position of Nomlaki Tuff, Radiometric date of 3.4 ± 0.3 Ma (Sarna-Wojcicki, 2000)	3
Pliocene	Repettian	Fernando / Repetto (Lower/Middle)	1st Anaheim		3500	Bentonite Marker Lower bathyal interbedded fine- to coarse grained sandstone, pebbly sandstone, sandy shale, siltstone, and claystone*	
Pliocene	Repettian	Fernando / Repetto (Lower/Middle)	2nd Anaheim		4000		
Pliocene	Repettian	Fernando / Repetto (Lower/Middle)	3rd Anaheim		4500		4
Miocene	"Delmon-tian"	A, B undiff.			5000	Upper to middle bathyal fine- to coarse-grained sandstone interbedded with sandy siltstone and platy siliceous siltstone with pebble conglomerate*	5 / 6
Miocene	Mohnian	C	Puente / Mohnian Shale		5500	Shale**	7
Miocene	Mohnian	D, E undiff.	Puente / Stem		6000 / 6500	Fine- to medium-grained sandstone and interbedded shale**	8

Arco Edwards 1 / Unocal Coyote 2-15

* - Based on Blake, 1991   ** - Based on proprietary oil industry data.

Figure 3: Type log and stratigraphy of East Coyote Hills oil field. Electric log picks based on oil industry data (left curve, spontaneous potential; right curve, resistivity) and West and Redin (1991). Benthic foram stages of Kleinpell (1938) and Miocene divisions of Wissler (1958) based on oil industry data and Blake (1991).
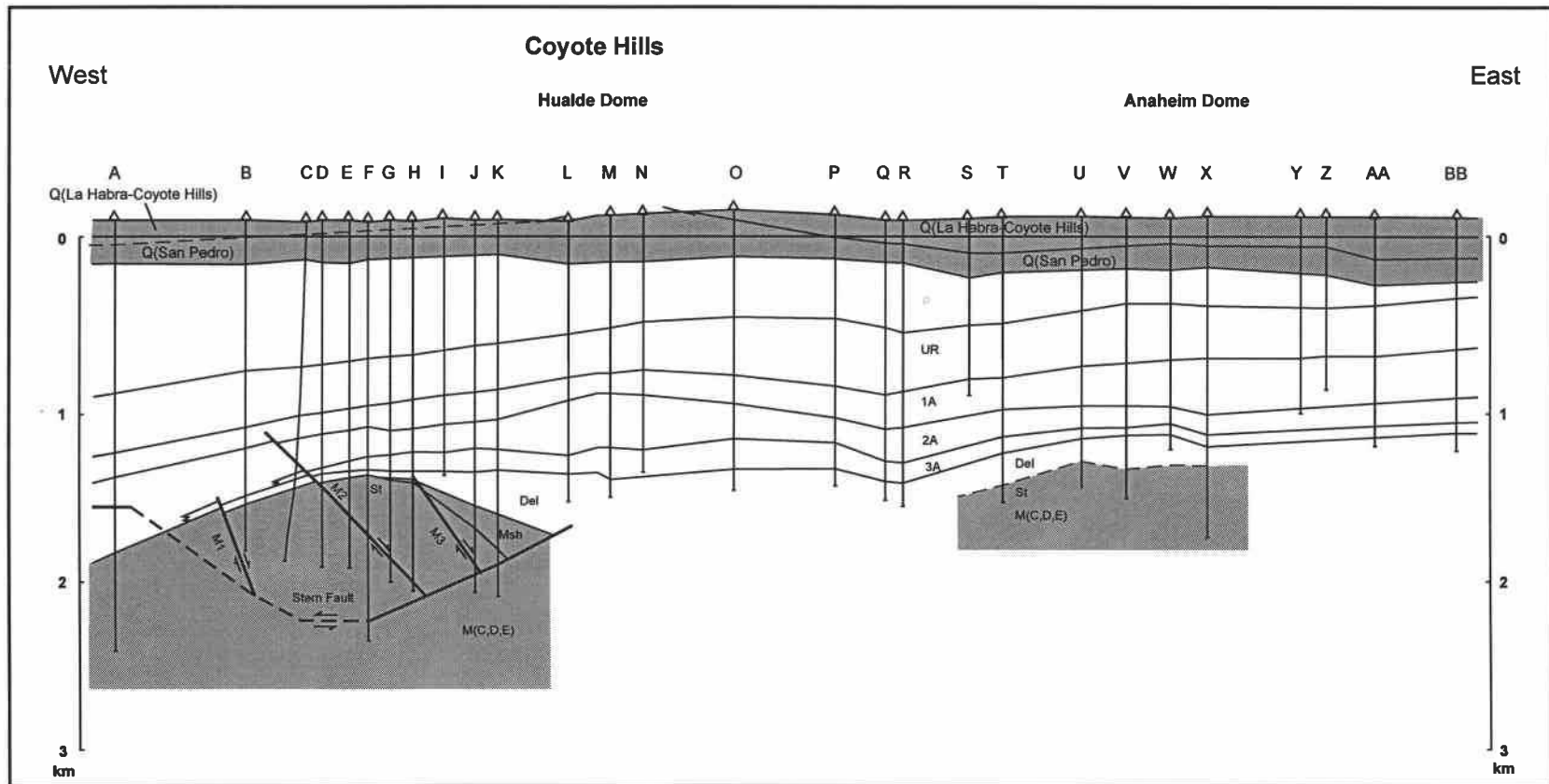
Figure 4: East-west cross section across the East Coyote oil field north of the Stern fault. Mohnian shale, "Delmontian" and 3rd Anaheim zone strata overlie Mohnian C, D and E along an angular unconformity. Pico strata (P) thin from west to east across the field. Extensive lateral thickness variations in the Repetto sands are present. Surface outcrop of the San Pedro- Coyote Hills contact from Tan et al. (1984).

Abbreviations are the same as for Figure 2. Wells identified in appendix.
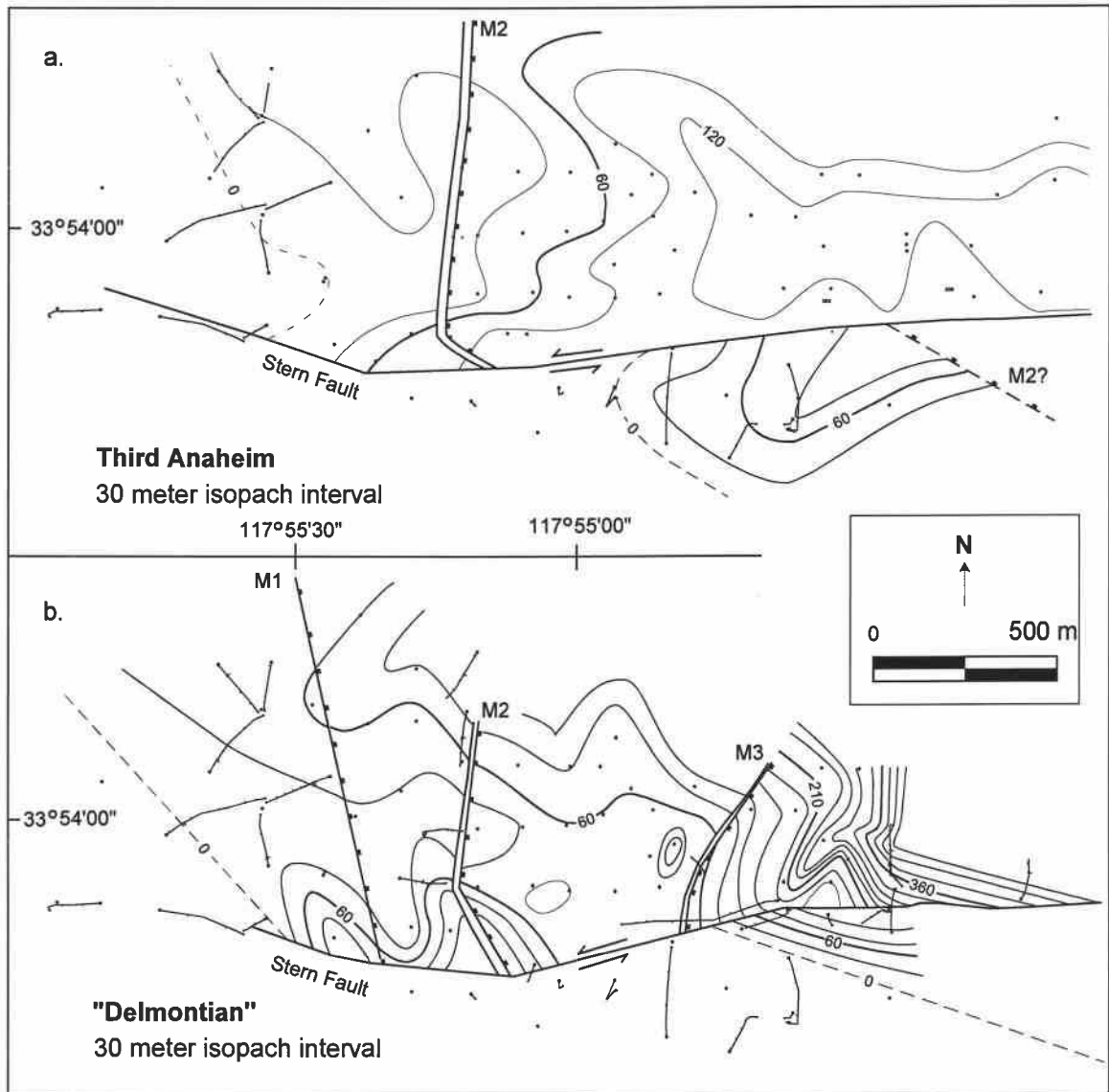
Figure 5: Isopachs of (a) 3rd Anaheim zone and (b) "Delmontian" strata . Pinchouts in both units are consistent with approximately 1200 m of left lateral offset on the Stern fault. Dots show well control with lines being the surface projections of directionally drilled wells. M1, M2 and M3 designate Miocene normal faults. For well names, see Map 106 of Division of Oil, Gas and Geothermal Resources (1998).

Formation are divided into the Third Anaheim, the Second Anaheim, and the First Anaheim oil producing zones. All are within the lower/middle Repetto undifferentiated sequence, the top of which is marked by a bentonite layer (located on Figure 3) that is very distinctive on electric logs and has been contoured in previous studies of the field (Ybarra and others, 1960). The upper Repetto consists of shale and sandy siltstone and contains a thick sandstone body, the Hualde zone (not present in the type log, Figure 3).

The upper Repetto-Pico contact shows up clearly on most electric logs as a transition from silty, shaly, and relatively sandstone-free strata of the upper Repetto to sandier siltstone of the Pico. Pico strata contain numerous discontinuous sandstone beds lacking in the upper Repetto. The Pico Member is of Pliocene and Pleistocene age.

Quaternary units in the East Coyote oil field include, in ascending order, the San Pedro, Coyote Hills, and La Habra formations, as well as Quaternary alluvial and colluvial deposits (Yerkes, 1972; Tan and others, 1984). The San Pedro Formation is composed of massive siltstone overlain by interbedded sandstone and siltstone (Powell and Stevens, 2000). Strontium age estimates of a mollusk within the San Pedro Formation yielded an age of 1.4 ± 0.4 Ma (Powell and Stevens, 2000). The only contact extensively traceable in the subsurface is the San Pedro-Pico contact. The contact appears on electric logs as a slight upward-widening funnel culminating in massive sandstone near the top of the San Pedro (Figure 3). The coarsening-upward sequence represents the transition from inner neritic to non-marine facies (Blake, 1991). The surface casings of most wells in the East Coyote field are below the San Pedro-Coyote Hills contact, and the section behind the surface casing is not logged. Accordingly, we were unable to contour this contact. On the Hualde dome section (Figures 2a and 4), the San Pedro-Coyote Hills contact is projected into the subsurface using the surface mapping of the contact by Tan and others (1984). We were unable to map the La Habra-Coyote Hills contact in the well logs, and therefore we do not differentiate between the La Habra and Coyote Hills formations in this study.

STRUCTURE

The Hualde and Anaheim domes of the East Coyote oil field differ in structure and topographic expression. The Hualde dome has topographic expression as low hills trending east-northeast (Figure 7). The structure of the upper Repetto within the Hualde dome also trends east-northeast, but the structure of older and younger strata trends east-west (Figure 6). The Anaheim dome trends east-west and has less topographic expression than the Hualde dome. The trend of the East Coyote Hills is strongly influenced by the southwest-flowing Brea Creek and Fullerton Creek and satellite tributaries (Figure 7). The anticline in the San Pedro Formation does not control this drainage, and we suggest that the drainage system is antecedent to uplift of the Coyote Hills. The domes are en-échelon, stepped-left with respect to each other. Both domes contain folded Quaternary strata (Figures 2 and 6a). Thinning of the Pico member and upper Repetto member, and little or no thinning of the middle-lower Repetto member across the crests of the anticlines indicate that fold growth began during the deposition of the upper Repetto (Figure 2). Both domes appear to be still growing. The reduced topographic expression of the Anaheim dome may be due to erosion by the Fullerton Creek drainage system as well as the larger Carbon Creek drainage, now diverted to the east (Figure 7). Another factor is the smaller structural relief of the Anaheim dome relative to the Hualde dome (Figure 2).

In order to determine the cause of folding of the East Coyote Hills, it is necessary to determine which structures within the East Coyote oil field are active and which are inactive. To accomplish this, we characterize the timing and offset of faults within the Hualde and Anaheim domes.

Hualde Dome

The Hualde dome shows three stages of deformation: Miocene-Pliocene normal faulting, then left-lateral oblique slip faulting on the Stern fault on the south flank of the Hualde dome, and, finally, folding of the Hualde dome. Three north-south striking

Miocene-early Pliocene normal faults cut strata as young as the Repetto member (Figures 4, 5a). These faults were undocumented by previous published work and were first
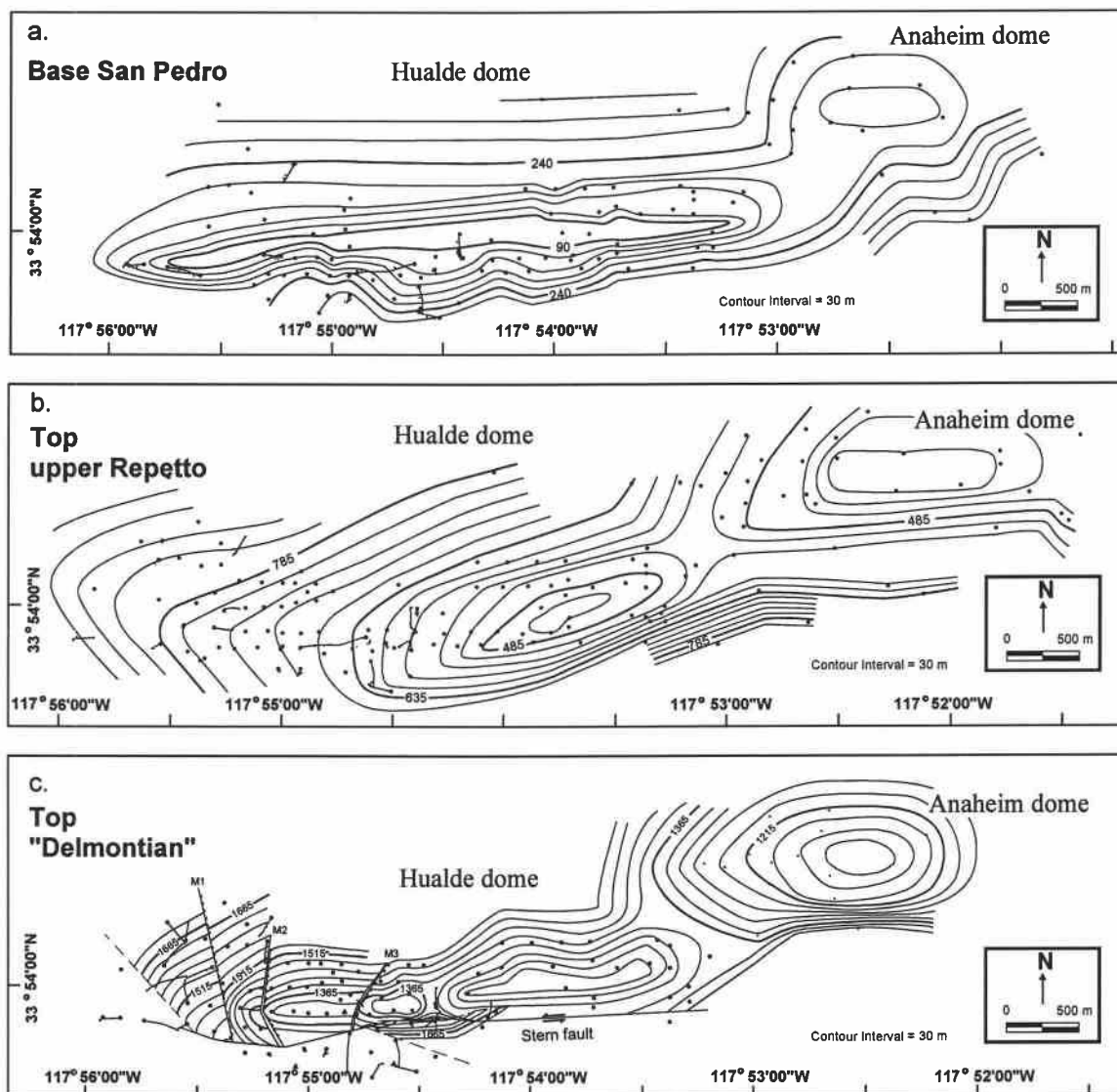
Figure 6: Structure contours of the (a) base San Pedro, (b) top Upper Repetto and (c) top "Delmontian" surfaces. All contour values are meters below sea level. The Hualde and Anaheim domes are both asymmetric with steeper south limbs and separate fold culminations. The Hualde dome has more steeply-dipping fold limbs than the Anaheim dome. Miocene normal faults are labeled M1, M2 and M3. Dots show well control with lines being the surface projections of directionally-drilled wells. For well names, see Map 106 of Division of Oil, Gas and Geothermal Resources (1998).
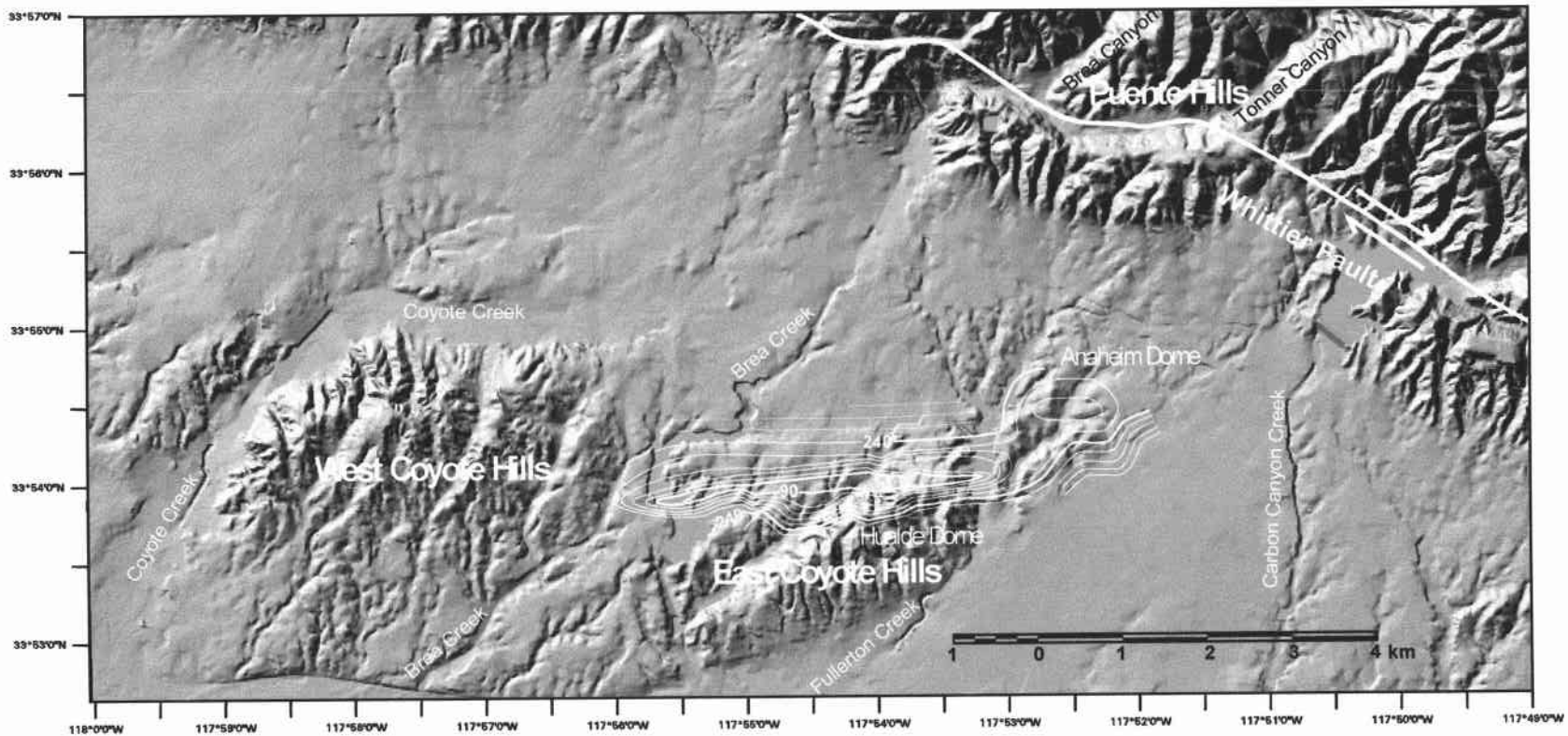
Figure 7: Topography, Pico structure contours, and geographic features of the Coyote Hills. The discord between the east-west trending fold structure and the east northeast trend of the East Coyote Hills is readily apparent. The shape of the East Coyote Hills is determined by erosion from a east northeast trending drainage on the northeast flank of the hills and possibly by Brea Creek. The subdued topographic expression of the Anaheim dome relative to the Hualde dome results from erosion of the Anaheim dome by Fullerton Creek and its tributaries as well as the lower structural relief of the Anaheim dome.

Topography created from US Geological Survey 30 meter digital elevation model.

described in a proprietary oil-industry study of the Hualde dome. In this study, the faults are designated, from west to east, as M1, M2, and M3 (Figure 5). We rechecked the fault cuts found in the oil industry study and recontoured several stratigraphic surfaces to verify the location of these faults. Well control on the faults is best north of the Stern fault and is relatively poor south of the Stern fault. Normal offsets on all three faults are about 30 meters. The M1 fault is based on offset of structure contours of the top of the Third Anaheim zone. We were unable to find M1 fault cuts in Hualde dome well logs. The M2 and M3 faults have recognizable fault cuts on well logs so that these faults could be contoured.

We cannot constrain the time of initiation of these normal faults, but faulting must have ceased during the time of deposition of the Repetto, with the M2 fault showing the youngest activity (Figure 4). This late "Delmontian"-early Repetto normal faulting corresponds in time to a general period of northwest-southeast extension in the Los Angeles basin (Wright, 1991).

South of the Stern fault, the Miocene normal faults are poorly constrained by well data. Wells along strike of the M2 and M3 faults do not show missing stratigraphic sections. This indicates that the Miocene-Pliocene normal faults are laterally offset by the Stern fault. Since the M2 fault does not appear in any of the wells south of the Stern fault, Mio-Pliocene normal faults must be offset at least 250 meters if offset along the Stern fault is right-lateral, and 1 km if offset along the Stern fault is left-lateral.

Stern Fault

The Stern fault strikes approximately east-west along the south flank of the Hualde dome (Figure 5). The Stern fault offsets strata as young as lower Pico. In the eastern portion of the Hualde dome, the Stern fault dips approximately 75 ° to the north at depths of 900 to 1200 m. It steepens with depth to approximately 85° to the north. In the western portion of the Hualde dome, the Stern fault has a more constant dip of approximately 75°, but still shows some steepening with depth. The fault is approximately normal to bedding (Figure 2a). Folding began after the fault became

inactive, indicating that the formerly-vertical fault was folded along with the Miocene and Pliocene strata it cuts.

Previous workers (Yerkes, 1972; Wright, 1991) mapped the Stern Fault as a high angle reverse fault with approximately 285 m of separation. More detailed work by oil industry geologists and ourselves indicates the Stern fault is a left-lateral oblique-slip fault with approximately 1100 ± 200 m of left lateral offset. Evidence for strike slip comes from several sets of offset structures and strata, as well as the general geometry of the fault itself.

As mentioned above, the Miocene-Pliocene normal faults are cut by the Stern fault. Though the normal faults are too poorly constrained south of the Stern fault to use them to quantify strike slip offset, their absence in wells south of fault requires a minimum offset of 1 km if the offset is left-lateral.

The stratigraphic evidence for left lateral offset is much stronger. Electric logs of strata north and south of the Stern fault do not correlate (Figure 2a). Pinchouts in the Third Anaheim zone and the "Delmontian" strata show left-lateral offset (Figure 5). To use stratigraphic pinchouts as piercing points to demonstrate lateral offset, one must first show that there is not a left jog in a submarine channel that could mimic left-lateral offset on the Stern fault. We consider this unlikely, however, because isopachs of the "Delmontian" strata show that a channel, if present, trends at high angles to the Stern fault, and no channel is found parallel to or close to the Stern fault (Figure 6).

Several stratigraphic units show abrupt thickness changes across the Stern fault that are inconsistent with reverse slip and are best explained by strike-slip offset. Figure 2a shows abrupt thickness changes in the First and Second Anaheim zones across the Stern fault. The "Delmontian" section is thick north of the Stern fault but absent south of the fault. Furthermore, the top of the Stern Zone shows apparent normal separation across the Stern fault. Alternatively, this could be explained by erosion of the top of the Stern Zone by a submarine canyon that is later filled with "Delmontian" strata, or by normal displacement on the Stern fault during deposition of the "Delmontian" strata followed by reactivation as a reverse fault. Neither of these explanations, however, is consistent with the absence of "Delmontian" strata south of the Stern fault.

The South Flank fault of the West Coyote oil field appears to be the continuation of the Stern fault. This correlation was rejected by Wright (1991) based on the geometry of the two faults based on the limited subsurface data available to him. Structure contours of the faults prepared by oil industry geologists and ourselves, however, align remarkably well (Figure 8). Abrupt thickness changes in "Delmontian" and Repetto strata across the South Flank fault also support the interpretation of strike slip on the South Flank fault (Figure 9). The South Flank fault is traced even farther west into the Leffingwell oil field (Figure 10), where it is not associated with a growing fold.

Anaheim Dome

The Anaheim dome contains no major faults. Ybarra and others (1960) mapped a small reverse fault on the south flank of the Anaheim dome. We were unable to map this fault in any of the wells adjacent to the well shown on the cross-section published by Ybarra and others (1960) that shows a repeated section. We found similar thickening at the same stratigraphic level in other nearby wells, suggesting that the apparent repeated section on the published cross-section is a stratigraphic effect. The mapped fault dips approximately 60° to the north, suggesting that, even if it exists, the fault is unlikely to be a continuation of the Stern fault which has a steeper dip. The absence of the Stern fault in the Anaheim dome suggests that the Stern-South Flank fault is not related to the folding. With 1100 ± 200 m of slip, the Stern-South Flank fault must continue to the east, but would be south of well control in the Anaheim dome, probably between wells C and D in Figure 2b.

The folded Quaternary strata in the Hualde and Anaheim domes indicate that these are active structures. Given the apparent left-lateral strike-slip nature of offset on the Stern fault and its steep dip, it seems unlikely that the Stern fault is responsible for the growth of the Hualde dome. Similarly, the absence of a major south flank fault on the Anaheim dome indicates that there is some other active structure responsible for the deformation of the Anaheim dome. We propose that the most likely structure, given the asymmetric, southward vergent geometry of the two domes, is a north dipping, blind reverse fault that does not cut wells in the East or West Coyote oil fields.
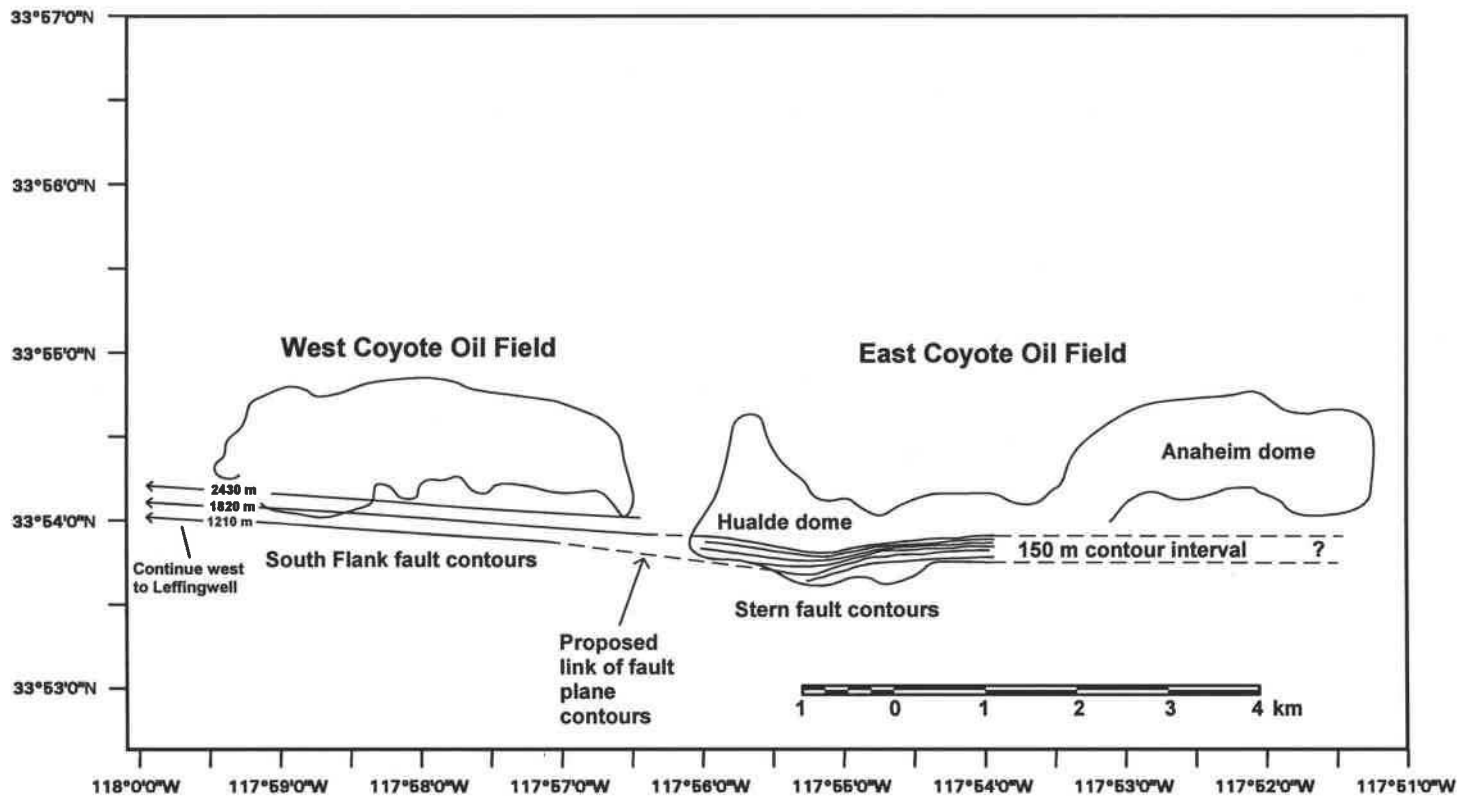
Figure 8: East and West Coyote oil fields and fault plane contours. Alignment of the South Flank and Stern fault plane contours suggests that they may be the same fault. The eastward projection of the fault is south of the Anaheim dome in an area without well control.
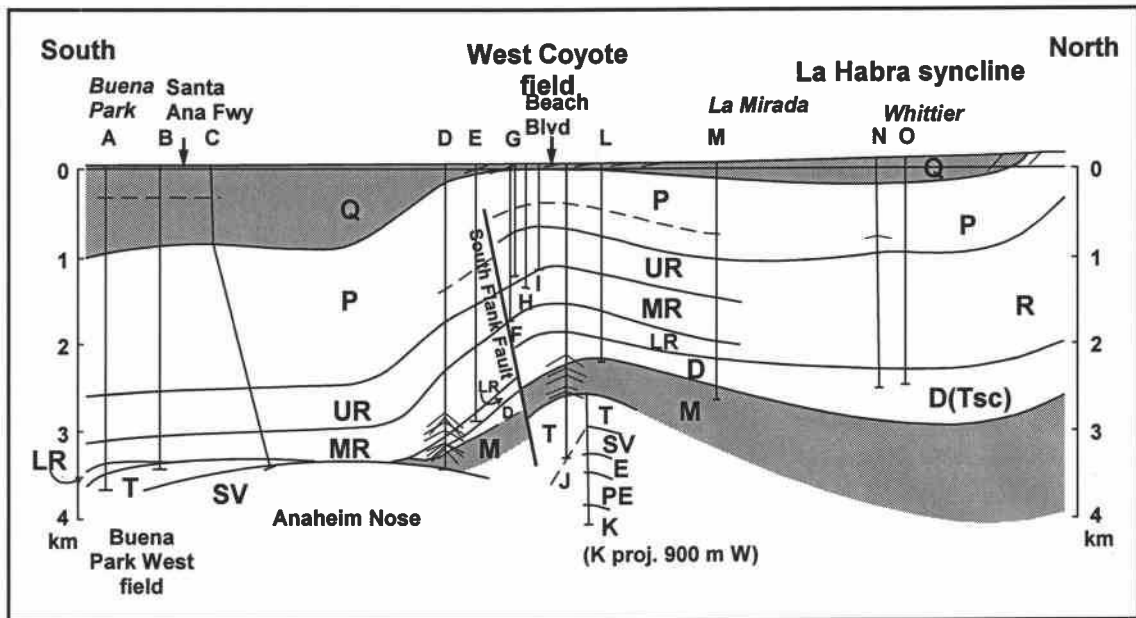
Figure 9: North-south cross section across West Coyote oil field. Note similarity in dip of the South Flank fault of West Coyote to that of the Stern fault of the Hualde dome of East Coyote. The relief on the base San Pedro surface is approximately 1000 m on this section, similar to the relief of this surface in the Hualde dome of East Coyote. The thickness of the lower Repetto and "Delmontian" changes abruptly at the fault. Abbreviations and symbols are the same as for Figure 2. Wells identified in appendix.
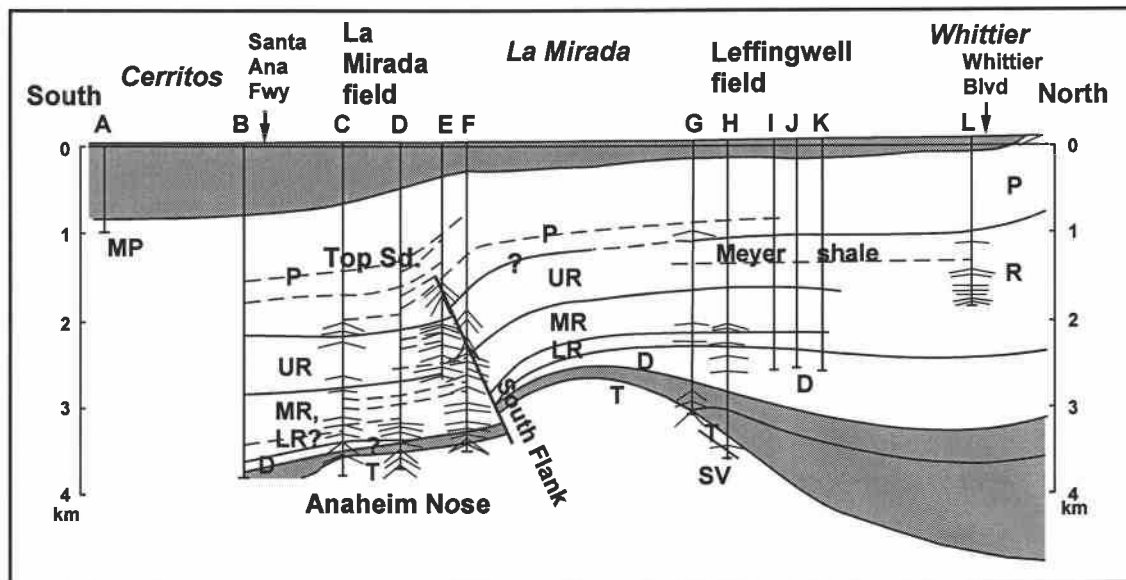
Figure 10: North-south cross section across the Leffingwell oil field. Relief on the base San Pedro surface has decreased to approximately 350 m indicating decreased displacement on the structure responsible for the folding. There is no topographic expression of the structure, in contrast to West Coyote. Abbreviations and symbols are the same as for Figure 2. Wells identified in appendix.

MODELING OF THE COYOTE HILLS FOLD

Given that the proposed fault does not cut any of the wells in the East or West Coyote fields, and that seismic reflection transects across the area are of too poor quality to image such a fault, the best way to constrain the geometry and displacement on the fault is to use a mechanical or kinematic model to try to reproduce the observed folding. We chose dislocation modeling based on its past success in studying blind reverse faults (Ward and Valensise, 1994; Benedetti and others, 2000).

We used the three-dimensional dislocation modeling software of Toda and others (1998), which is based on Okada's (1994) theoretical formulation. The dislocation is placed in a homogeneous half-space. The Coyote Hills structure formed over a period longer than a million years during which most of the shear stress has been relaxed. To simulate complete shear relaxation of the lithosphere, the shear modulus is set to zero, following Ward (1986). The effect of assuming relaxed moduli on the shape of the fold is minor.

Identifying the fault plane that best reproduces the observed folding of the Coyote Hills requires fitting for six fault parameters: (1) depth of the upper fault tip, (2) horizontal location of the upper fault tip, (3) depth of the lower fault tip, (4) fault length, (5) fault dip, and (6) fault displacement (Figure 11). Lack of data and details of the modeling procedure limit the number of parameters that can realistically be determined.

Relief on the fold is constrained by wells far from the Coyote oil fields. Strata at these locations are approximately equidistant from the West Coyote field and the Hualde and Anaheim domes of the East Coyote oil field. Strata in distant wells have been affected by deformation from all three structures. To model the deformation completely, it is necessary to allow variation in the geometry and displacement of three faults independently, one underlying each dome. We simplify the problem by modeling the folding of East and West Coyote Hills using a single fault underlying both folds, although in reality, the fault might be segmented. A consequence of this simplifying assumption is that evaluating model fit in 3-dimensions is unnecessary. Instead, the fit of the model to the observed fold is evaluated by comparing a profile of the model fold across its crest to

a north-south profile across the Coyote Hills structure. The model fault is assumed to strike east-west based on the east-west trend of the East Coyote structures (Figure 6a). Since the East and West Coyote folds have similar shapes and relief (Figures 2a and 9), we fit only the Hualde dome of East Coyote.

Unique determination of the best-fit fault length and depth to the lower fault tip is not possible based on a single profile because varying the depth to the lower fault tip of the fault and varying the fault length produce similar effects on the model profile (Figure 12). Shallowing the lower fault tip or shortening the fault length both result in reductions of fold amplitude and wavelength perpendicular to the strike of the fold that are similar in magnitude. Because subsurface well data provide some constraint on the length of the fault from the along-strike extent of folding, we choose to fix that parameter of the model. Relief on subsurface folds east of the Hualde dome and west of the West Coyote oil field rapidly decreases (Figures 2b and 10), suggesting that a fault 7.3 km long extending from the western edge of West Coyote to the eastern edge of the Hualde dome is a reasonable approximation and probably represents a lower limit of fault length.

We take a grid-search approach, considering many possible combinations of dip, location of upper fault tip, fault width, and displacement. Goodness of model fit to the chosen stratigraphic surface is evaluated using a reduced least-squares difference method. A stacked Hualde dome profile is created by projecting all of the well picks for a deformed stratigraphic surface within the Hualde dome and in wells outside of the East Coyote field onto a north-south vertical plane (Figure 13). Data points at the crest of the fold are assigned weights approximately equal to half the width of the cluster of data points at the crest. This reflects the uncertainty in the fold amplitude created by collapsing the points of a dome-shaped surface onto a north-south vertical plane. Data points on the flanks of the fold are assigned weights based on the error in making the log picks and are roughly an order of magnitude smaller than the errors of the points on the crest of the fold. Therefore, points on the flanks are weighted more heavily than points on the crest in determining goodness of fit. We modeled the deformation of the Pico-San Pedro contact. Results from modeling this surface suggest that deeper stratigraphic surfaces are probably cut by the fault responsible for the folding and cannot be used to constrain the fault geometry.
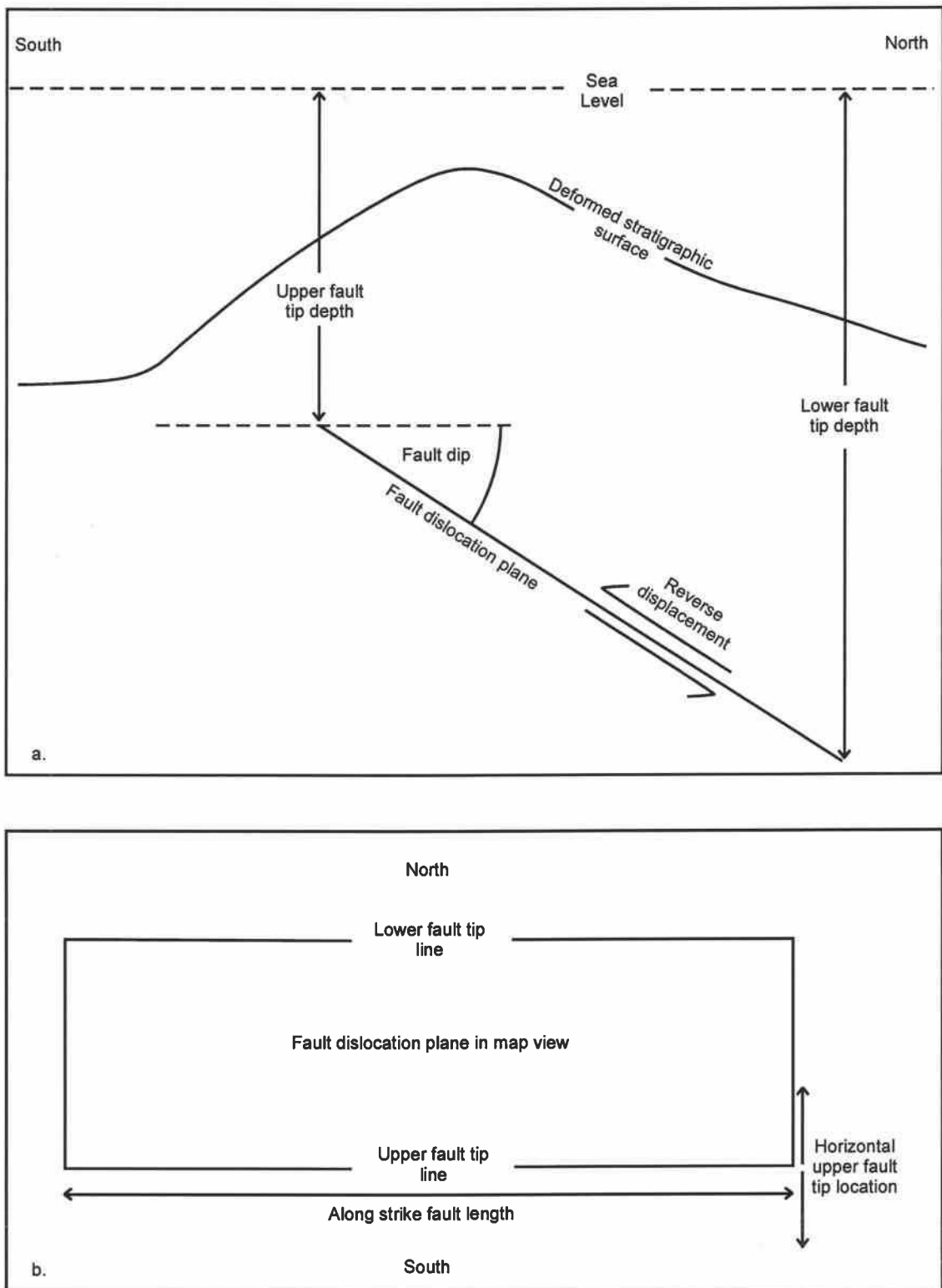
Figure 11: Dislocation model parameters. a) Cross sectional view showing fault dip, upper fault tip depth, lower fault tip depth, and displacement. b) Map view of fault plane showing along strike fault length and horizontal upper fault tip location.
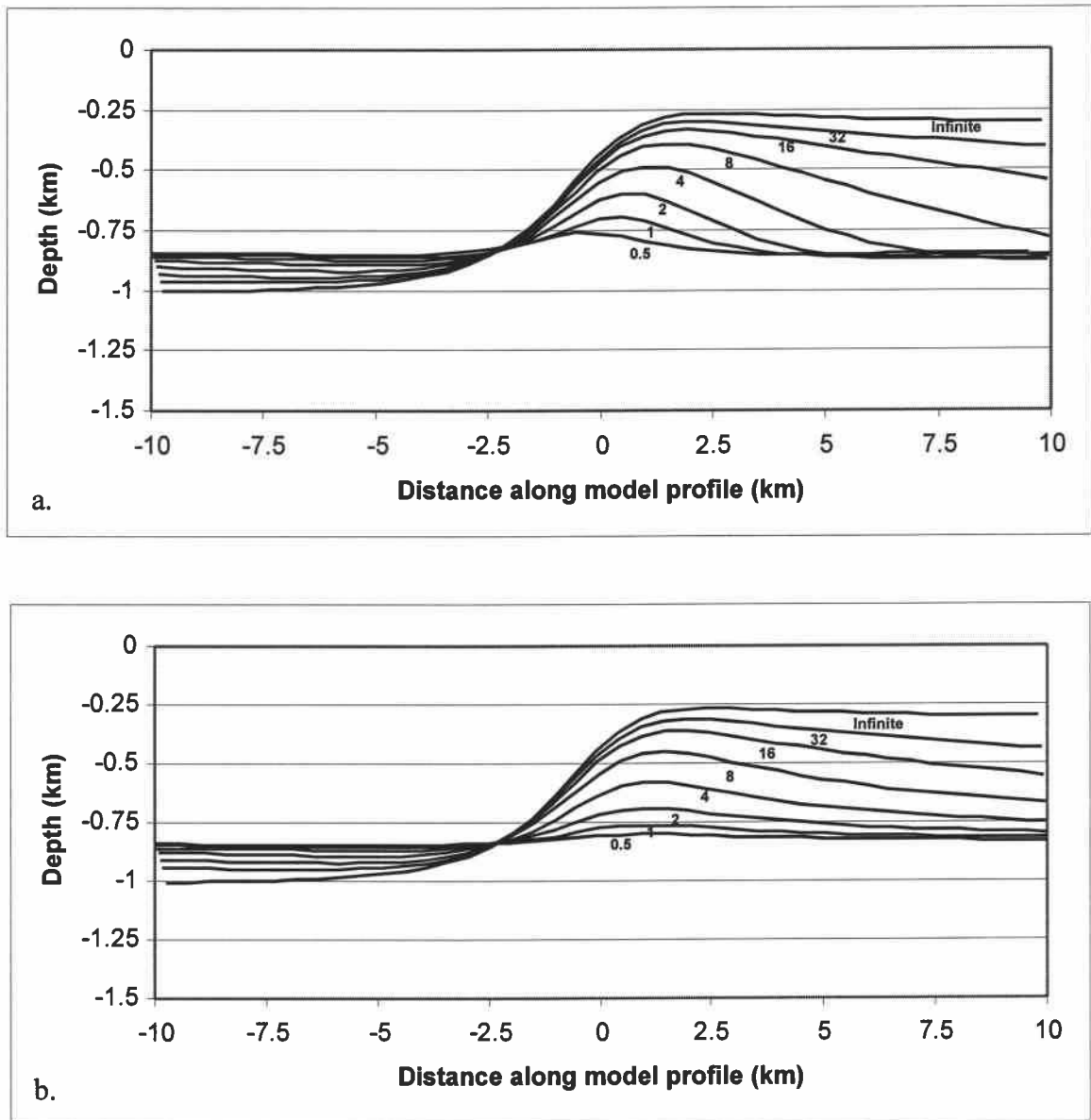
Figure 12: The response of a dislocation model to variations in a) the depth of the lower fault tip depth and b) fault length along strike. Changing the lower fault tip depth and fault length produce similar effects on fold amplitude and wavelength. Fitting for both parameters in a dislocation model is therefore difficult. Because well data provide some constraint on the width of the blind thrust fault beneath the Coyote Hills, that parameter was held constant in the grid searches. Faults in the above figures dip 45 degrees to the positive x-axis direction, have a reverse displacement of 1000 m, have an upper fault tip depth of 3 km, and a horizontal upper fault tip location at 0 km along the x-axis. The y-axis denotes depths below the surface of the model half-space. Individual profiles are labeled with a) depth of the lower fault tip and b) fault length in km.
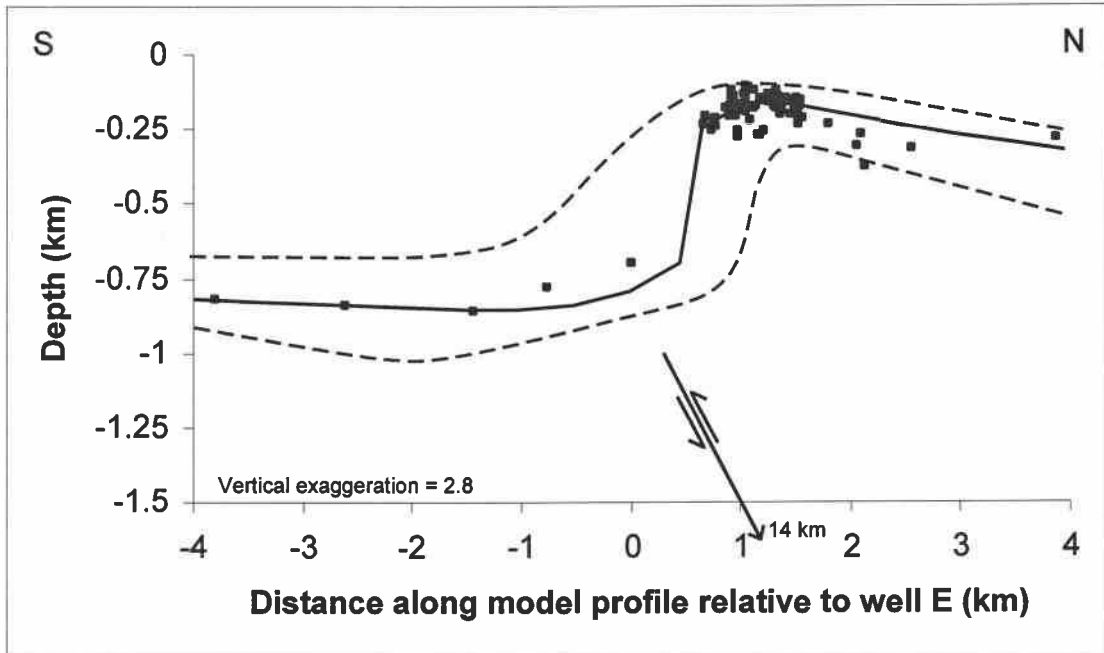
Figure 13: Best least-squares fit dislocation model. Squares show the projection of the Pico-San Pedro boundary control points onto a north-south plane. The fault producing the model shown has a dip of $35°$ $^{+50°}/_{-20°}$ N, reverse displacement of 1400 $^{+1500}/_{-500}$ m, an upper fault tip depth of 1 $^{+2}/_{-1}$ km, a horizontal top tip location of 0.3 $^{+1.3}/_{-0.4}$ km north of well E of Figure 2a, a lower fault tip depth of 14 $^{+?}/_{-11}$ km, and a length of 7.3 km. Asymmetric errors on best-fit parameters denoted using forward slash. The best-fit fault is shown on the plot. Dashed lines represent boundaries of statistically acceptable profiles within a 68% confidence interval. No geologic constraints are placed on a profile's acceptability.

The best-fit fault based on modeling the Pico-San Pedro contact has a dip of 35° $^{+50°}/_{-20°}$ N, reverse displacement of 1400 $^{+1500}/_{-500}$ m, an upper fault tip depth of 1 $^{+2}/_{-1}$ km, a horizontal top tip location of 0.3 $^{+1.3}/_{-0.4}$ km north of well E of Figure 2a, a lower fault tip depth of 14 $^{+∞}/_{-11}$ km, and a length of 7.3 km (Figures 13, 14, 15, and 16). The errors in Figures 14,15 and 16 represent 68% confidence intervals on a 5-parameter delta chi squared error space (Press et al., 1986).

Changes in one model parameter are compensated by changes in another parameter. This effect severely increases the uncertainty with which model parameters are resolvable. Figure 14 demonstrates the tradeoff in best-fit displacement with changes in upper fault tip depth. Increasing upper fault tip depth requires an increase in reverse displacement to achieve an acceptable fit. A wider range of acceptable displacements and upper fault tip depths accompany an increase in the fault dip. This is because at greater dips where most of the displacement goes into producing vertical uplift, the shape of the fold becomes less sensitive to increasing displacement. Only the amplitude changes with increasing displacement, which in turn can be compensated for by increasing the upper fault tip depth. Because of these tradeoffs and the lack of well data on the south flank of the Hualde dome, the model places only weak constraint on the fault dip.

The maximum lower fault tip depth limit cannot be estimated. Grid searches deeper than 16 kilometers for the lower fault tip depth do not produce appreciable changes in the fold shape at the wavelength of the Coyote Hills fold (Figure 12). Furthermore, depths much greater than 15 kilometers are likely to be below the seismogenic zone of the Los Angeles basin (Hauksson and Haase, 1997).

Figure 17 shows a north-south cross section across the Hualde dome redrawn with the best-fit dislocation fault. The upper fault tip depth, lower fault tip depth and horizontal fault location are within the errors of the best-fit dislocation model. Having the thrust fault cut the upper Repetto (UR) is consistent with abrupt thickness changes within the upper and middle-lower Repetto (MR, LR) on the south flank of the Hualde dome that were shown as stratigraphic thickening without a fault in Figure 2a.
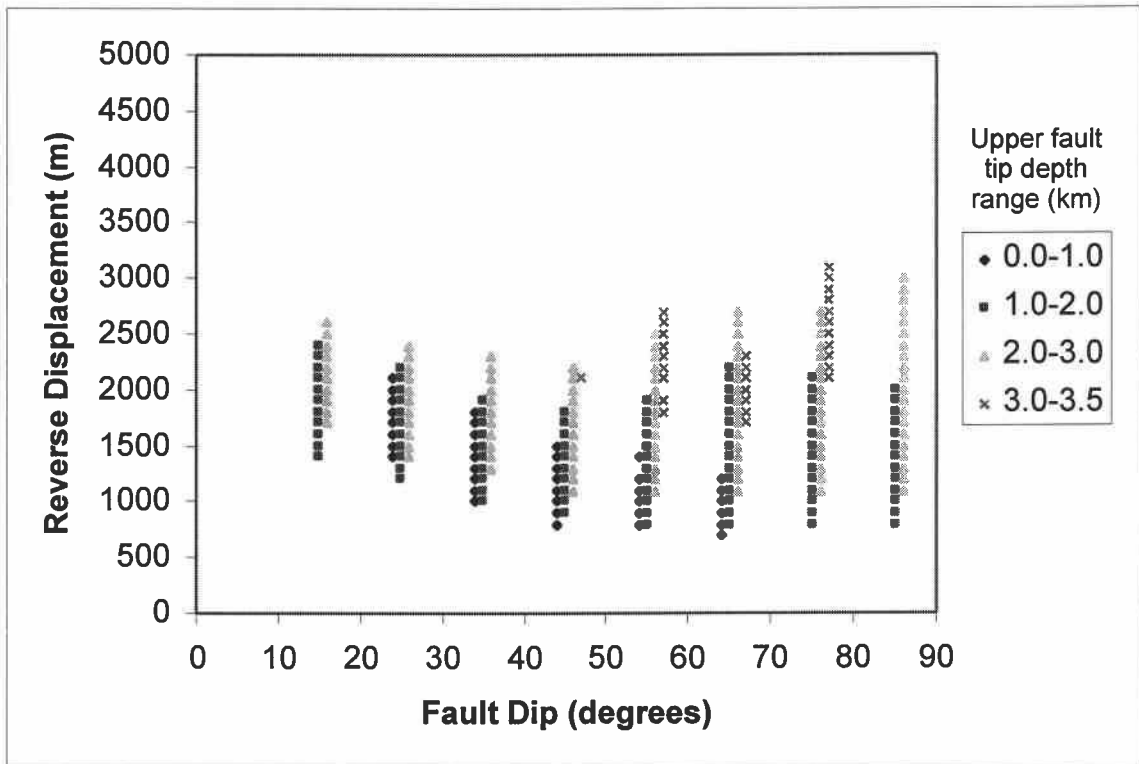
Figure 14: 68 % confidence intervals of the 5 parameter space for fault dip and reverse displacement for fitting a fault to the Pico-San Pedro boundary. Each group of models is categorized by upper fault tip depth (see explanation) to demonstrate the interplay among fault dip, reverse displacement and upper fault tip depth. For each dip, faults with deeper upper tips require larger offsets to achieve an optimal fold fit. More steeply dipping faults produce statistically acceptable fits over a wider range of reverse displacements. Groups of points with constant upper fault tip depths have been offset artificially along the dip axis so that the groups do not completely overlap. Groups are centered on dips of 15, 25…85 degrees.
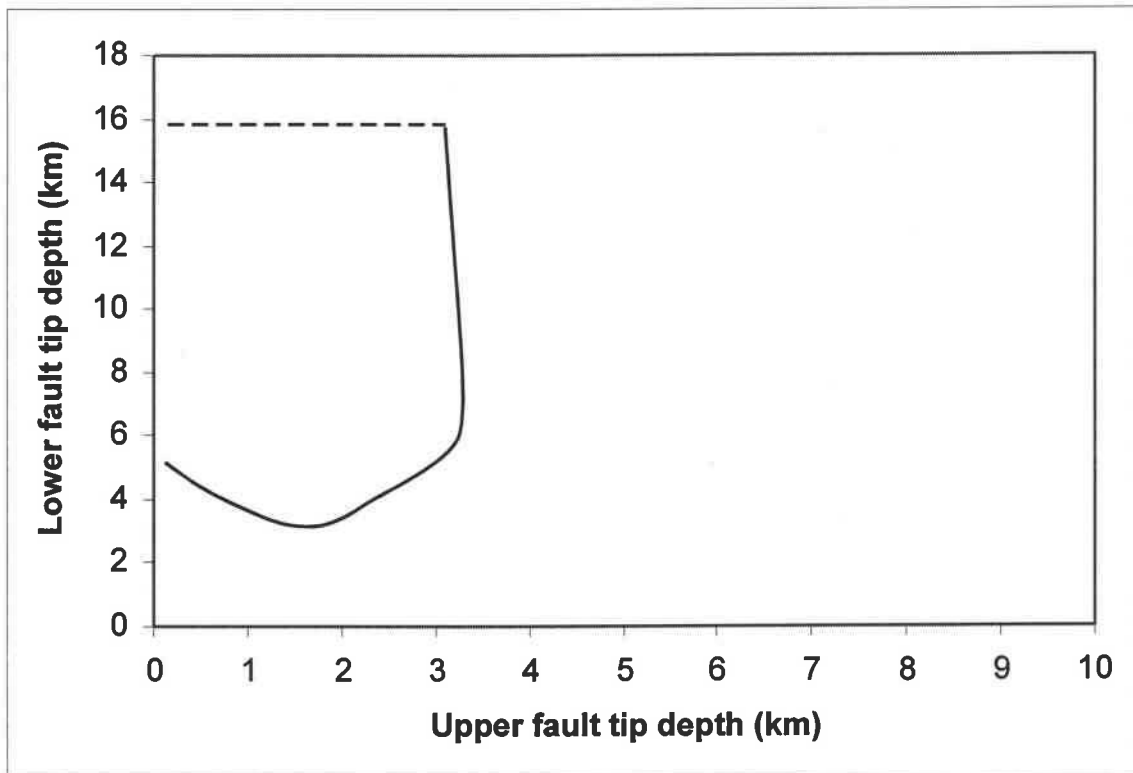
Figure 15: 68 % confidence intervals of the 5 parameter space for upper fault tip depth and lower fault tip depth for fitting a fault to the Pico-San Pedro boundary. Fault producing statistically acceptable fits have upper fault tip depths ranging from 0 km to 3.2 km and lower fault tip depths as shallow as 3.2 km. An upper bound on lower fault tip depth could not be found due to the reduced effect of the lower fault tip on the fold geometry as the lower fault tip deepens. The dashed line on the graph represents the maximum depth for the lower fault tip used in the dislocation models.
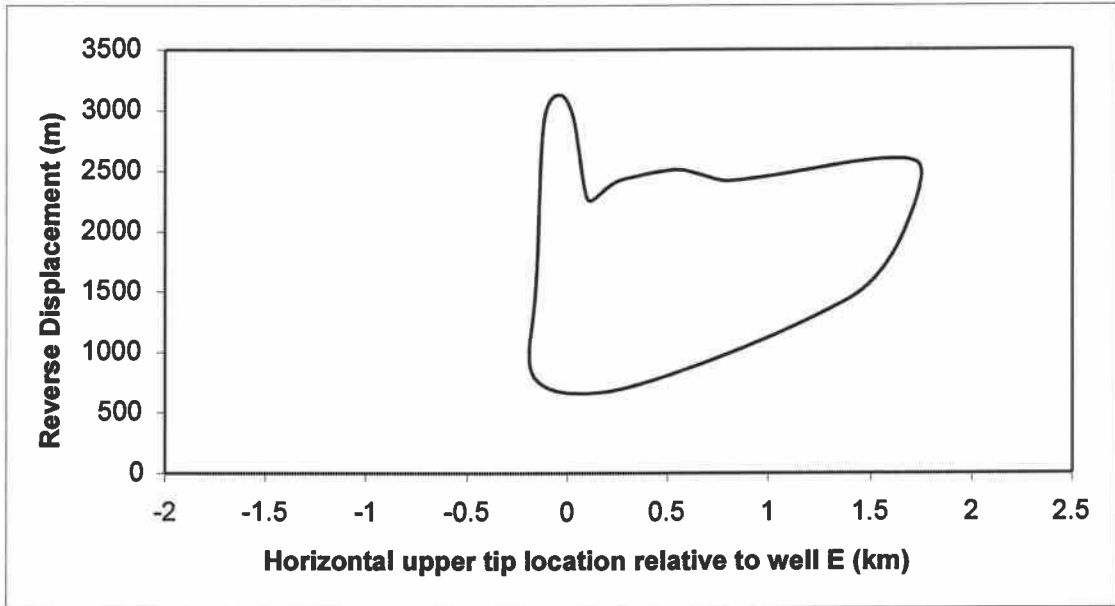
Figure 16: 68 % confidence intervals of the 5 parameter space for horizontal upper fault tip location and reverse displacement for fitting a fault to the Pico-San Pedro boundary. The origin of the horizontal location axis is on well E of Figure 2a. Horizontal upper fault tip distances in the above graphs are distances north (+) or south (-) of well E of Figure 2a.
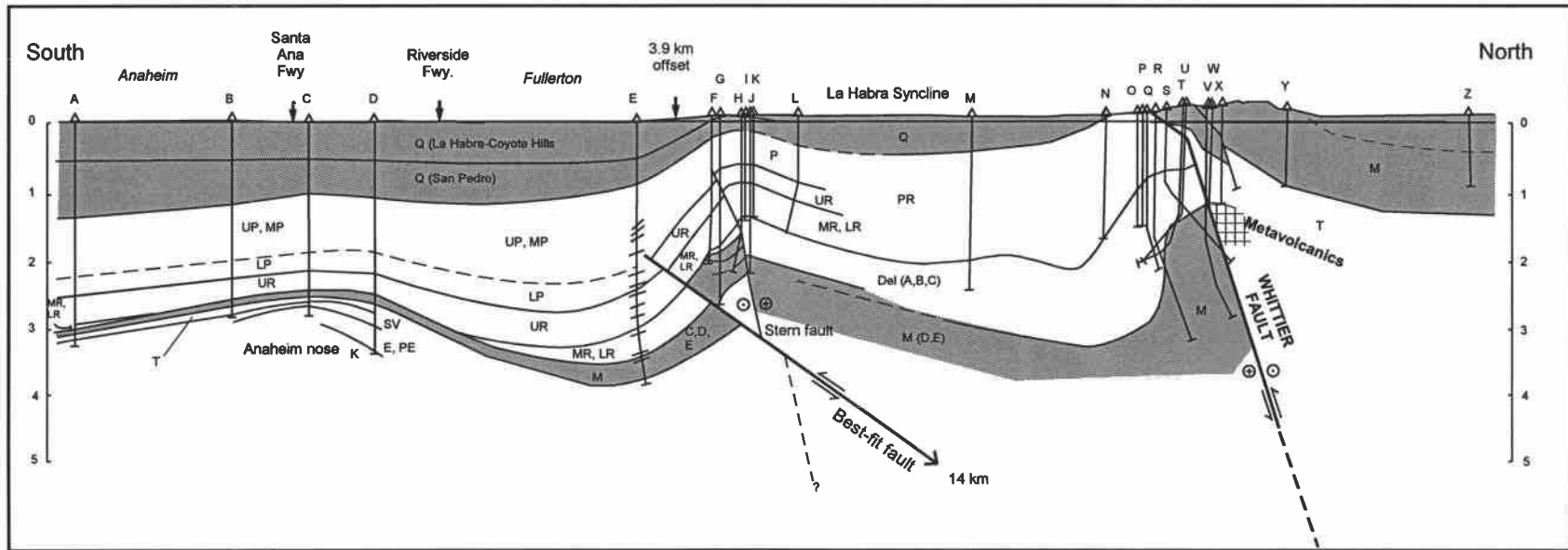
Figure 17: North-south cross section of Figure 2a redrawn with 35° dipping thrust fault and geology north of Whittier fault. Upper fault tip depth, lower fault tip depth and horizontal fault location are within the errors of the best-fit dislocation model. Having the thrust fault cut the upper Repetto (UR) is consistent with abrupt thickness changes within the upper and middle-lower Repetto (MR, LR) on the south flank of the Hualde dome that were shown as stratigraphic thickening without a fault in Figure 2a. Geology of the Whittier fault and area to the north by Tom Bjorklund. Abbreviations and symbols are the same as for Figure 2. Wells identified in appendix.

AGE CONSTRAINTS AND SLIP RATES

Ages for the Pico-San Pedro and upper Repetto-Pico contacts are determined by linearly interpolating between the Brunhes-Matuyama magnetic chron boundary and the Nomlaki tuff. An additional constraint is the 1.4 ± 0.4 Ma age estimate of a mollusk in the San Pedro Formation in the West Coyote Hills (Powell and Stevens, 2000). Cores taken from a water well located at 34.0014 ° N, 118.07673 ° W by D. Ponti and others (e-mail comm., 2000) indicate that the magnetic polarity of the sediments changes from normal at 73.3 m depth to reversed at 133.9 m. A base San Pedro type electric log signature in this water well occurs at 149.1 m, indicating that the Brunhes-Matuyama chron boundary lies within the San Pedro Formation. The Nomlaki tuff is correlated by electric log to well C on Figure 18 based on its occurrence just above the Meyer shale in the Union Bell 60 well in the Santa Fe Springs oil field. The age of the Brunhes-Matuyama chron boundary is estimated at 780 ± 10 ka (Spell and others, 1992). The Nomlaki tuff is dated at 3.4 ± 0.3 Ma by Sarna-Wojcicki and others (1991) based on the K-Ar method. The well depth below sea level of the Brunhes-Matuyama boundary and Nomlaki tuffs in well C on Figure 18 are 104 ± 30 m and 1364 ± 10 m, respectively. Based on a depth of 317 m for the Pico-San Pedro surface, linear interpolation between the Brunhes-Matuyama boundary and the Nomlaki tuff yields an age of 1.2 ± 0.1 Ma for the Pico-San Pedro boundary surface (Figure 19). The Sr-isotope age estimate of 1.4 ± 0.4 Ma of a mollusk in the San Pedro formation is consistent with this age interpolation, although the Pico-San Pedro boundary may be older at East Coyote than it is in the section depicted on Figure 18. Based on these ages and the best-fit displacements calculated from the dislocation model, we calculate a slip rate of $1.2 \, ^{+1.4}/_{-0.5}$ mm/yr.
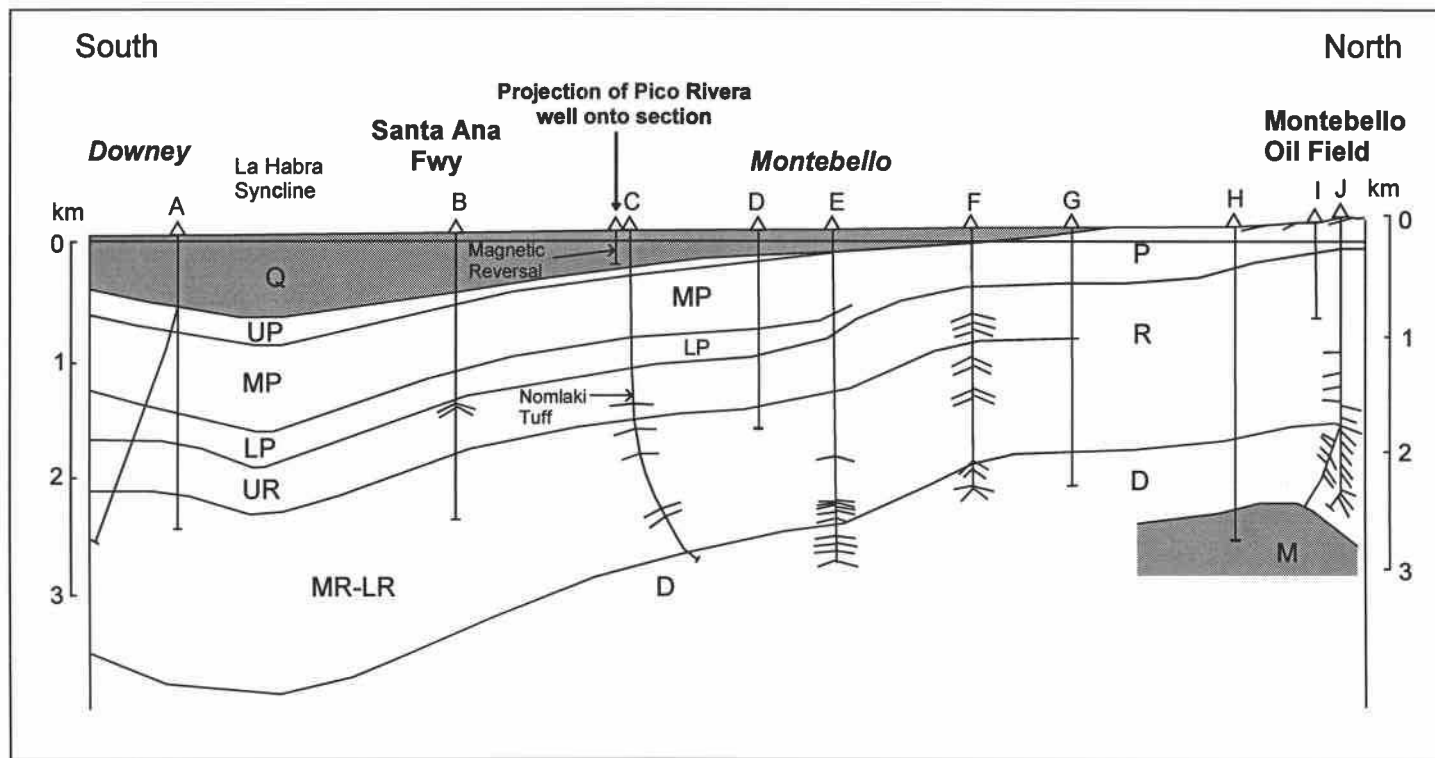
Figure 18: North-south cross section from Montebello oil field to Downey, west of Santa Fe Springs oil field, showing the projection of the Pico Rivera water well onto the cross section and the approximate location of the Brunhes-Matuyama boundary relative to the base San Pedro surface. The Nomlaki tuff is correlated to well C (Shell Pansini 1) by electric log from the Union Bell 60 well in the Santa Fe Springs oil field.
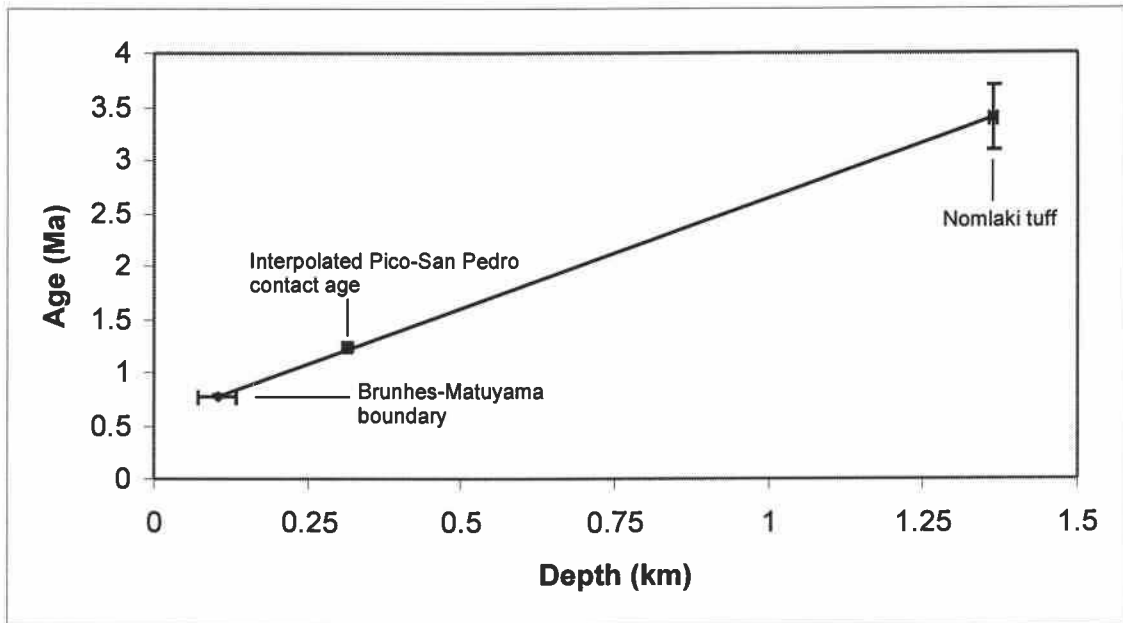
Figure 19: Age determination of the Pico-San Pedro boundary. The Brunhes-Matuyama boundary and Nomlaki tuffs have ages 780 ± 10 ka (Spell and others, 1992) and 3.4 ± 0.3 Ma (Sarna-Wojcicki and others, 1991) respectively. The depths of the Brunhes-Matuyama boundary and Nomlaki tuffs on Figure 18 are 104 ± 30 m and 1364 ± 10 m respectively. Taking depths of 317 m for the base San Pedro surface and 1140 m for the top of the upper Repetto and linearly interpolating between the Brunhes-Matuyama boundary and the Nomlaki tuff yields an age of 1.2 ± 0.1 Ma for the base San Pedro surface.

DISCUSSION

Relation of Coyote Hills Thrust to Other Structures to the North

The thrust fault beneath the Coyote Hills has important implications for Los Angeles basin seismic hazard and tectonics. Shaw and Shearer (1999) suggested that a large system of thrust faults underlies the Puente Hills and the northern Los Angeles basin based on oil-industry seismic data. The Puente Hills thrust fault, constrained by fault-plane reflections on a seismic profile, location of the mainshock and aftershocks of the 1987 Whittier Narrows earthquake, and a fault-plane solution for the mainshock, dips 25° to the north and has an upper fault tip depth of 3 km (Shaw and Shearer, 1999). The thrust fault beneath the Coyote Hills may be an extension of the Puente Hills thrust based on the similarities of dip and upper fault tip depth between the Puente Hills thrust and the best fit dislocation model for the thrust fault beneath the Coyote Hills (Figure 20). Shaw and Shearer (1999) also show the beginning of offset structure contours to the east of the Santa Fe Springs oil field.

Under this scenario, the Coyote Hills thrust becomes part of a major crustal feature. The best-fit dislocation fault and the projection of the Whittier fault creates an intersection at approximately 10 km depth (Figure 21). This is the depth of intersection obtained by Fuis et. al. (2001) when they projected the Puente Hills thrust and Whittier faults downward. Fuis et al (2001) suggested that the Puente Hills thrust shallows to a 10° N dipping detachment based on the LARSE I crustal profile, a detachment that they suggest terminates in the San Andreas fault zone (Figure 21). This model suggests that slip is partitioned among the Coyote Hills thrust, the Whittier fault, and the Sierra Madre fault. The Sierra Madre and Coyote Hills thrust take up the reverse component of slip, and the Whittier fault takes up the right-lateral component of slip. Previous studies and the uplift of the Puente Hills suggest that the Whittier fault has a component of reverse displacement. This component, however, is likely to be small due to the absence of an axial fold surface north of the Whittier fault (Figure 17). Alternatively, some of the uplift of the Puente Hills may result from deformation within the block between the Whittier and Sierra Madre faults.
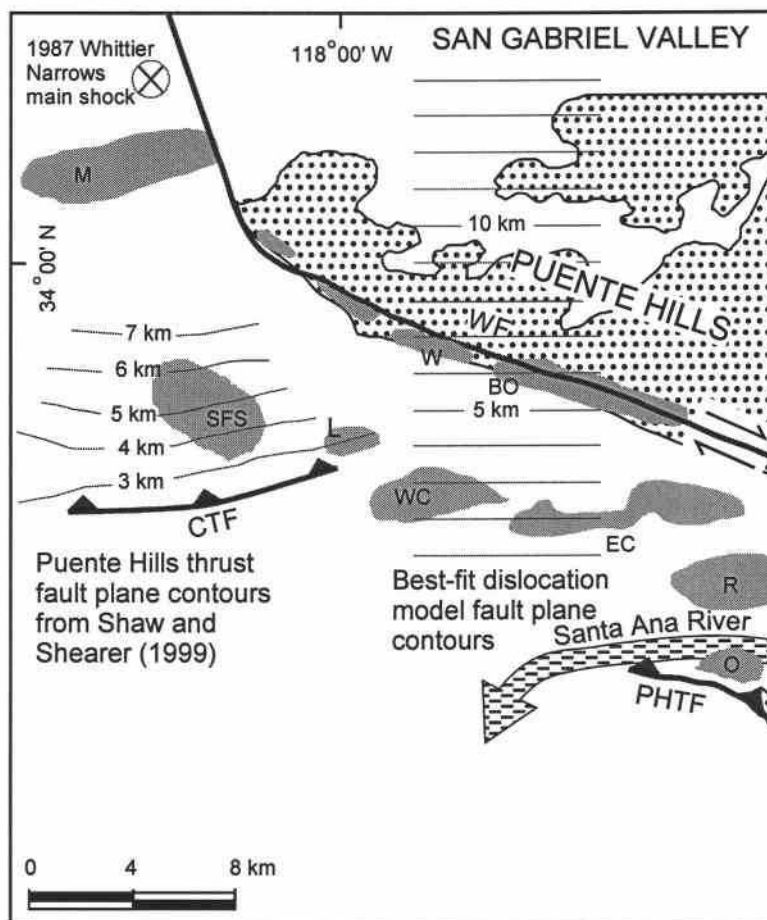
Figure 20: Fault plane contours for the best-fit dislocation fault for the Coyote Hills blind thrust and the Puente Hills thrust (Shaw and Shearer, 1999). Similarity in dip and upper fault tip depth between the Puente Hills thrust and the Coyote Hills thrust suggest that they are part of the same fault system. The Carmenita thrust fault of the petroleum industry (CTF) is equivalent to the Puente Hills thrust of Shaw and Shearer (1999). Abbreviations are the same as in Figure 1.
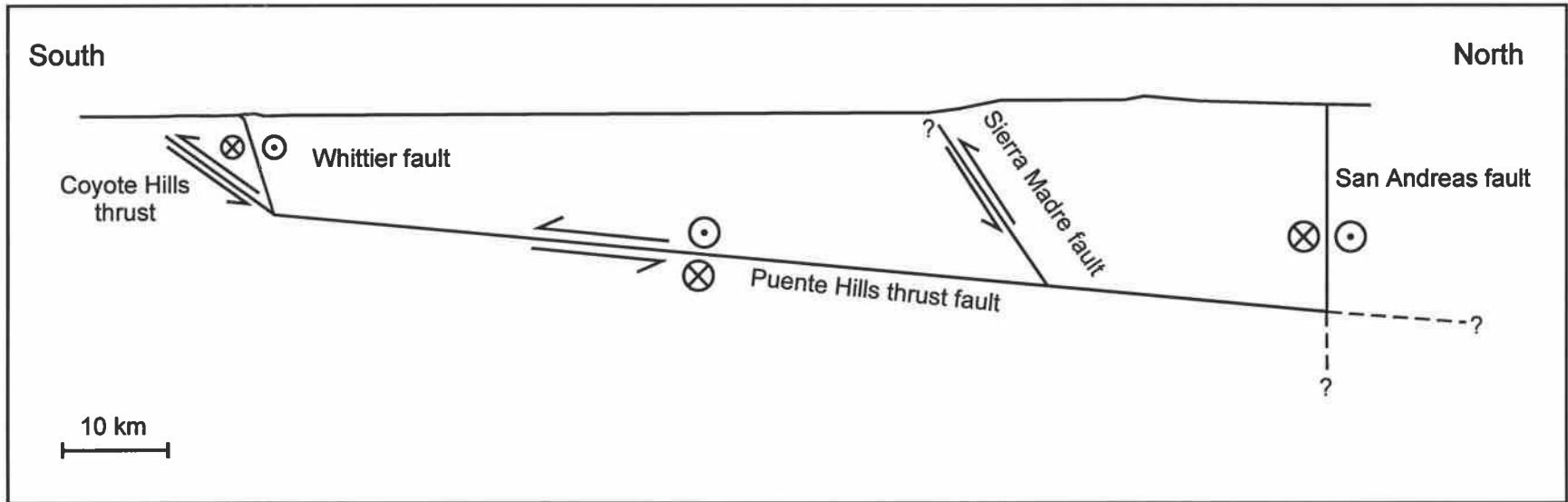
Figure 21: Schematic cross section showing the relation of the Coyote Hills thrust to the Whittier fault, the Puente Hills blind thrust, the Sierra Madre fault, and the San Andreas fault. The Whittier fault and the thrust fault beneath the Coyote Hills are projected to their point of intersection at approximately 10 km depth. This value is similar to the depth of intersection obtained for the intersection between the Whittier fault and the Puente Hills thrust based on deep seismic profile, LARSE 1, (Fuis et al, 2001) suggesting that the Puente Hills thrust and the thrust beneath the Coyote Hills are part of the same thrust system.

Relating the Slip Rate of the Coyote Hills Thrust to Other Structures

The slip rates calculated for the Whittier-Elsinore fault show a decrease from southeast to northwest. Along the Glen Ivy segment of the northern Elsinore fault just south of its junction with the Chino fault (Figure 1a), Gath et. al. (1988) determined a horizontal slip rate of 6 mm/yr at Glen Ivy. Just north of the intersection of the Coyote Hills trend with the Whittier fault, the horizontal slip rate is 2-3 mm/yr (Rockwell et al., 1992; Gath and Gonzalez, 1995). Based on these differences, Rockwell et al (1992) suggested that 3 mm/yr could be taken up on the Chino fault, although Heath et al (1982) estimated a slip rate of only 0.8 mm/yr on the Chino fault. The remaining 1 mm/yr may be taken up by the thrust fault beneath the Coyote Hills and by deformation within the footwall of the Whittier fault, the latter illustrated by the footwall anticline in the Brea-Olinda oil field shown in Figure 17.

Seismic Hazard

Knowing the slip rate and approximate geometry of the fault allows the calculation of the potential earthquake moment magnitude that could be generated by the Coyote Hills blind thrust and the recurrence interval for such an earthquake. The 1994 Northridge and 1987 Whittier Narrows earthquakes, which both occurred on blind thrust faults in the Los Angeles Basin, had static stress drops of 100 bars (Abercrombie and Mori, 1994) and 155 ± 43 bars (Lin and Stein, 1989), respectively. A stress drop of 100 bars is assumed for the Coyote Hills blind thrust. Assuming a circular rupture on the fault, the seismic moment can be calculated from the stress drop using the equation obtained by Keilis-Borok (1959)

$$M_0 = 16/7R^3\Delta\sigma,$$

where R is the radius of rupture and $\Delta\sigma$ is the stress drop . If the model fault ruptures along its entire length of 7.3 km, then R = 3.6 km, and $M_0 = 1.1 \times 10^{18}$ N-m. This yields a moment magnitude of $M_w = 6.0$. If $\mu = 3 \times 10^{10}$ Nm^{-2} and the expression $M_0 = \mu Ad$ (Burridge and Knopoff, 1964) is solved for d, where A is the rupture area and d is the

average slip on the fault during the earthquake, then d = 0.88 m. Using a slip rate of 1.2 mm/yr, the recurrence interval for a M_w = 6.0 earthquake is 730 years.

If the Coyote Hills thrust is part of the larger Puente Hills thrust system, then an earthquake might rupture both the Coyote Hills segment and the segment beneath the Santa Fe Springs oil field as a cascade, though this did not happen during the 1987 Whittier Narrows earthquake. In this scenario, the length of the fault becomes 24 km. Figure 12 suggest that we should correct the estimated slip rate due to the increase in the fault length. Based on Figure 12, an increase in fault length from 7.3 km to 24 km brings approximately a 50% increase in fold amplitude. Since fold amplitude is linearly related to displacement in the dislocation model, we decrease the fault displacement by a factor of 0.64 to 900 m. When combined with the age estimate of 1.2 Ma for the Pico-San Pedro boundary, the slip rate becomes 0.8 mm/yr.

Assuming a dip of 25° for the fault based on the results of Shaw and Shearer (1999) for the Whittier Narrows source fault and assuming that the fault ruptures to 13 km depth as it did in the 1987 Whittier Narrows earthquake, the fault would have a down-dip width of 27 km. Taking R = 13 km in the above equation and using a stress drop of 100 bars yields M_0 = 5.0 x 10^{19} N-m. This yields M_w = 7.1, d = 3.2 m, and an average recurrence interval of 4000 years.

CONCLUSION

The Coyote Hills of the Los Angeles basin are the expression of active folding, but this folding is unrelated to the Stern fault of the East Coyote oil field or the South Flank fault of the West Coyote oil field. Based on offset pinchouts of Delmontian and Repetto strata and truncated Miocene-Pliocene normal faults within the Hualde dome of the East Coyote oil field, the Stern fault is a strike-slip fault with 1100 ± 200 m of left-lateral offset. Movement on the Stern fault ended sometime during the beginning of deposition of the Pico Member of the Fernando Formation, prior to folding of the Coyote Hills anticline. Well data do not support the presence of a major south flank fault along the Anaheim dome of the East Coyote oil field; the fault is probably located south of the field. Fault plane contours of the South Flank fault of the West Coyote oil field and the Stern fault of the East Coyote oil field suggest that they are the same fault. This fault continues west to the Leffingwell oil field and probably continues eastward south of the Anaheim dome of the East Coyote oil field. The strike-slip nature of the Stern-South Flank fault and the absence of a major south flank fault in the Anaheim dome suggest that the Stern-South Flank fault predates the folding and that a blind thrust that does not cut oil wells in any of the oil fields is responsible for the active folding of the Coyote Hills.

Dislocation modeling of the observed folding of a stratigraphic surface in the Hualde dome of the East Coyote field suggests that the blind thrust fault has a dip of $35°$ $^{+50°}/_{-20°}$ N, reverse displacement of $1400 \, ^{+1500}/_{-500}$ m, an upper fault tip depth of $1 \, ^{+2}/_{-1}$ km, a horizontal top tip location of $0.3 \, ^{+1.3}/_{-0.4}$ km north of well E of Figure 2a, a lower fault tip depth of $14 \, ^{+\infty}/_{-11}$ km, a length of 7.3 km, and a slip rate of $1.2 \, ^{+1.4}/_{-0.5}$ mm/yr averaged over the last 1.2 Ma. A fault length of 7.3 km is assumed based on the lengths of the East and West Coyote subsurface folds.

The dip and upper fault tip depth suggest that the thrust fault beneath the Coyote Hills is a continuation of the Puente Hills thrust system. This link between the two faults has important implications for the tectonics and earthquake hazards of the Los Angeles basin. The Coyote Hills-Puente Hills blind thrust system may play a role in the partitioning of slip among faults southwest of the San Andreas Fault. The amount of slip

taken up by the Coyote Hills-Puente Hills thrust system has implications for the slip on the Chino fault.

The potential moment magnitude for an earthquake on the Coyote Hills blind thrust with the above parameters is in the range of 6 - 7. The magnitude depends on whether or not a rupture on the Coyote Hills blind thrust would propagate westward to the segment of the Puente Hills thrust responsible for the 1987 Whittier Narrows earthquake. Recurrence intervals range from 730 to 4000 years depending on the estimated moment magnitude used to determine average slip on the fault during an earthquake and on the slip rate.

BIBLIOGRAPHY

Abercrombie, R. and J. Mori, Stress drops of the Northridge mainshock and larger aftershocks, Seismological Research Letters 65, p 243, 1994.

Benedetti, L., P. Tapponnier, G.C.P. King, B. Meyer, I. Manighetti, Growth folding and active thrusting in the Montello region, Beneto, northern Italy, Journal of Geophysical Research 105, 739-766, 2000.

Blake, G.H., Review of the Neogene biostratigraphy and stratigraphy of the Los Angeles basin and implications for basin evolution, In: Biddle, K.T. (ed), Active margin basins, American Association of Petroleum Geologists Memoir 52, pp. 135-184, 1991.

Burridge, R., and L. Knopoff, Body force equivalents for seismic dislocations, Bulletin of the Seismological Society of America 54, 1875-1888, 1964.

Division of Oil, Gas and Geothermal Resources, Map 106: Brea-Olinda – East Coyote, 1998.

Durham, D.L., and R.F. Yerkes, Geology and oil resources of the eastern Puente Hills area, southern California, U.S. Geological Survey professional paper 420-B, 62 p., 1964.

Fuis, G.S., T. Ryberg, J.J. Godfrey, D.A. Okaya, J.M. Murphy, Crustal structure and tectonics from the Los Angeles basin to the Mojave Desert, southern California, Geology 29, 15-18, 2001.

Gath, E.M., J.H. Hanson, B.R. Clark, T.K. Rockwell, The Whittier fault in southern California: preliminary results of investigations, EOS 69, 260, 1988.

Gath, E.M. and T. Gonzales, Transtensional faulting with long recurrence intervals through thte Whittier Narrows area, Rosemead, California: SCEC Annual Meeting, 55-56, 1995.

Gray, C.H., Geology of the Corona South Quadrangle and the Santa Ana Narrows area, Riverside, Orange, and San Bernardino counties, California, California Div. Mines Bull. 178, 5-58, 1961.

Heath, E.G., Jensen, D.E., and D.W. Lukesh, Style and age of deformation on the Chino fault, In: Cooper, J.D. (ed.), Neotectonics in southern California: Geological Society of America Cordilleran Section, Volume and Guidebook, 43-51, 1982.

Hauksson, E., J.S. Haase, Three-dimensional V_P and V_P/V_S velocity models of the Los Angeles basin and central Transverse Ranges, California, Journal of Geophysical Research 102, 5423-5453, 1997.

Keilis-Borok, V.I., On the estimation of the displacement in an earthquake source and of source dimensions, Annali di Geofisica 12, 205-214, 1959.

King, G.C.P., R.S. Stein, J.B. Rundle, The growth of geological structures by repeated earthquakes, Journal of Geophysical Research 93, 13307-13318, 1988.

Kleinpell, R.M., Miocene stratigraphy of California, American Association of Petroleum Geologists, 450 p., 1938.

Lin, J., and R.S. Stein, Coseismic folding, earthquake recurrence, and the 1987 source mechanism at Whittier Narrows, Los Angeles Basin, California, Journal of Geophysical Research 94, 9614-9632, 1989.

Okada, Y., Internal deformation due to shear and tensile faults in a half-space, Bulletin of the Seismological Society of America 84, 935-953, 1994.

Powell, C. L. and D. Stevens, Age and paleoenvironmental significance of meg-invertebrates from the "San Pedro" Formation in the Coyote Hills, Fullerton and Buena Park, Orange County, Southern California, U.S. Geological Survey open-file report 00-319, 83 p., 2000.

Press, W.H., B.P. Flannery, S.A. Tuekolsky, W.T. Vetterling, Numerical recipes: The art of scientific computing, Cambridge University Press, pp. 818, 1986.

Rockwell, T.K., E.M. Gath, and T. Gonzalez, Sense and rate of slip on the Whittier fault zone, eastern Los Angeles basin, California, Proceedings of the 35th Annual Meeting of the Association of Engineering Geologists, p. 679, 1992.

Sarna-Wojcicki, A.M., Lajoie, K.R., Meyer, C.E., Adam, D.P., Rieck, H.J., Tephrochronologic correlation of upper Neogene sediments along the Pacific margin, conterminous United States, The Geology of North America K-2, 117-140, 1991.

Shaw, J.H. and P.M. Shearer, An elusive blind-thrust fault beneath metropolitan Los Angeles, Science 283, 1516-1518, 1999.

Spell, T.L., I. McDougall, Revisions to the age of the Brunhes-Matuyama boundary and the Pleistocene geomagnetic polarity timescale, Geophysical Research Letters 19, 1181-1184, 1992.

Tan, S.S., R.V. Miller, J.R. Evans, Environmental geology of parts of the La Habra, Yorba Linda, and Prado Dam quadrangles, Orange County, California, California

Department of Conservation: Division of Mines and Geology Open-File Report 84-24, 1984.

Toda, S., R.S. Stein, P.A. Reasenberg, J.H. Dieterich, A. Yoshida, Stress transferred by the 1995 $M_w = 6.9$ Kobe, Japan, shock: Effect on aftershocks and future earthquake probabilities, Journal of Geophysical Research 103, 24543-24565, 1998.

Ward, S.N., A note on the surface volume change of shallow earthquakes, Geophysical Journal of the Royal Astronomical Society 85, 461-466, 1986.

Ward, S.N., G. Valensise, The Palos Verdes terraces, California: Bathtub rings from a buried reverse fault, Journal of Geophysical Research 99, 4485-4494, 1994.

West, J.C. and T.W. Redin, Correlation section across eastern Los Angeles basin from San Pedro Bay to San Gabriel Mountains, Pacific Section American Association of Petroleum Geologists, 1991.

Wissler, S.G., Correlation chart of producing zones of Los Angeles basin oil fields, *in* J.W. Higgins, ed., A guide to the geology and oil fields of the Los Angeles and Ventura regions: Pacific Section, American Association of Petroleum Geologists, p. 59-61, 1958.

Wright, T.L., Structural geology and tectonic evolution of the Los Angeles basin, California, In: Biddle, K.T. (ed), Active margin basins. American Association of Petroleum Geologists Memoir 52, pp. 35-134, 1991.

Ybarra, R.A., M.W. Dosch, A.D. Stockton, East Coyote oil field, In: Summary of operations of California oil fields vol. 64, Department of Natural Resources: Division of Oil and Gas, pp. 71-78, 1960.

Yerkes, R.F., Geology and oil resources of the western Puente Hills area, southern California, U.S. Geological Survey professional paper 420-C, 63 p., 1972.

Appendix

List of wells on cross sections.

Figure 2a

Well Letter	Well Name	Location
A	Chevron Kellogg 1, orig. hole	20-4S-10W
B	Amerada Anaheim Community 48	8-4S-10W
C	Texaco Anaheim Community A13-1	8-4S-10W
D	Conoco Anaheim Community 4-1	5-4S-10W
E	Quinn Edgington 1	29-3S-10W
F	Unocal Hole 63	23-3S-10W
G	Unocal Hole 61	22-3S-10W
H	Unocal Hole 65	23-3S-10W
I	Unocal Hole 45	23-3S-10W
J	Unocal Hole 23	23-3S-10W
K	Unocal Hole 21	23-3S-10W
L	M A. Cox Arroues 1	15-3S-10W
M	Hamilton and Sherman Union-Stewart Fee 54-10	10-3S-10W
N	Seacoast Wardman Community 1	2-3S-10W

Figure 2b

Well Letter	Well Name	Location
A	Occidental Ehrle 1	2-4S-10W
B	Royalty Service H-B 1	36-3S-10W
C	Rheem Placentia Fruit Co. 1	25-3S-10W
D	Utility Pet. Co. Strain 1	24-3S-10W
E	S. W. Bardford Smith 1	24-3S-10W
F	Unocal Gilman 1	24-3S-10W
G	Texaco Anaheim Union Water B 12	13-3S-10W
H	Texaco Anaheim Union Water B 2	13-3S-10W
I	Texaco Anaheim Union Water B 3	13-3S-10W
J	Texaco Anaheim Union Water B 8	13-3S-10W
K	Texaco Anaheim Union Water B 5	13-3S-10W
L	Texaco Anaheim Union Water B 7	13-3S-10W
M	Unocal Graham-Loftus 61-12	12-3S-10W

Figure 4

Well Letter	Well Name	Location
A	Unocal Sunny Hills 2-1	21-3S-10W
B	Unocal Sunny Hills 6	22-3S-10W
C	Unocal Sunny Hills 7	22-3S-10W
D	Unocal Toussau 3	22-3S-10W
E	Unocal Toussau 4	22-3S-10W
F	Unocal Toussau 2	22-3S-10W
G	Unocal Stern Realty 16	22-3S-10W
H	Unocal Stern Realty 11	22-3S-10W
I	Unocal Stern Realty 2	22-3S-10W
J	Unocal Coyote 2-15	22-3S-10W
K	Unocal Coyote 2-18	22-3S-10W
L	Unocal Hole 41	23-3S-10W
M	Unocal Hole 43	23-3S-10W
N	Unocal Hole 38	23-3S-10W
O	Unocal Hole 34	23-3S-10W
P	Unocal Anaheim Union Water 43	24-3S-10W
Q	Pyramid Anaheim Union Water 17	24-3S-10W
R	Pyramid Anaheim Union Water 21	24-3S-10W
S	Unocal Anaheim Union Water 15	24-3S-10W
T	Texaco Anaheim Union Water 8	13-3S-10W
U	Texaco Anaheim Union Water C-3	13-3S-10W
V	Texaco Graham-Loftus 58	13-3S-10W
W	Texaco Graham-Loftus Perkins 6	13-3S-10W
X	Unocal Graham-Loftus 59	18-3S-10W
Y	Unocal Graham-Loftus 18	18-3S-10W
Z	Unocal Graham-Loftus 19	18-3S-10W
AA	Pyramid Robertson 10	18-3S-10W
BB	Pyramid Johnson 4	18-3S-10W

Figure 8

Well Letter	Well Name	Location
A	Mobil Heath 2	34-3S-11W
B	Mobil Heath 1	34-3S-11W
C	Chevron Pacific Community 1	26-3S-11W
D	General Exploration Emery 1	24-3S-11W
E	General Exploration Emery-McNally 1	24-3S-11W
F	Derby Butch 1	24-3S-11W
G	Chevron Emery 98	24-3S-11W
H	Chevron Emery 114	24-3S-11W
I	Chevron Emery 112	24-3S-11W
J	Chevron Emery 87	13-3S-11W
K	Chevron Murphy Coyote 373	13-3S-11W
L	Chevron Emery 100	13-3S-11W
M	Union Stern 1	12-3S-11W
N	Branch Hi Lo Cinnabar 1	1-3S-11W
O	Dewey Livingston 1	1-3S-11W

Figure 9

Well Letter	Well Name	Well Location
A	California Western Koolhaas 1	29-3S-11W
B	Texaco Clanton 1	27-3S-11W
C	Mobil Librown 1	21-3S-11W
D	Texaco McNally 1-36	22-3S-11W
E	Texaco McNally A-1	22-3S-11W
F	Mobil McNally 1	15-3S-11W
G	Chevron German Community 1	11-3S-11W
H	Pyramid (Hathaway) Woodward Community K-1	11-3S-11W
I	Hathaway Woodward 2	11-3S-11W
J	Rothschild Woodward 1	11-3S-11W
K	Rothschild Fouquet 1	11-3S-11W
L	Santa Fe East Whittier Community 4-1	34-2S-11W

Figure 15

Well Letter	Well Name	Well Location
A	Chevron-Otto Community 1	35-2S-12W
B	Hathaway-Rossi 1	22-2S-12W
C	Shell-Pansini 1	23-2S-12W
D	Empire-Gaffey 1	4-2S-12W
E	ARCO Flood Control 1	14-2S-12W
F	Br. American-Pico 1	13-2S-12W
G	Whittier Narrows-Beverly Rd. Op. Unit 1	12-2S-12W
H	Chevron-Scott Inv. 1	1-2S-12W
I	Chevron-Baldwin 110	1-2S-12W
J	Chevron-Baldwin 72	1-2S-12W

Figure 17 (north of Figure 2a)

Well Letter	Well Name	Well Location
O	Cal. Resources Puente B-5	34-2S-10W
P	Cal. Resources Puente B-14	34-2S-10W
Q	Cal. Resources Puente B-9	34-2S-10W
R	Cal. Resources Puente B-7	34-2S-10W
S	Cal. Resources Puente B-8	34-2S-10W
T	Cal. Resources Puente B-28	34-2S-10W
U	Cal. Resources Puente B-32	34-2S-10W
V	Rowland Puente A-3	34-2S-10W
W	Cal. Resources Puente A-3	34-2S-10W
X	Cal. Resources Puente A-6	34-2S-10W
Y	Shell Puente C.H. 2	27-2S-10W
Z	H.O. Shively 1	23-2S-10W